

Materials and Environmental Circumstance: And All is Always Now

Jesús Toribio

Department of Materials Engineering, University of Salamanca, Spain

toribio@usal.es

Keywords: Environmentally assisted cracking, Hydrogen assisted cracking, Crack growth kinetics curve, K -dominance condition, Role of the far field, Effect of history.

Abstract. This paper offers a summary of the author's contributions in the field of fracture, damage tolerance and microstructural integrity of materials in a hydrogen environment. Paraphrasing the famous sentence by Ortega y Gasset "yo soy yo y mi circunstancia", one could say that *the material is itself and its circumstance*, the latter being the physico-chemical and mechanical environment. The paper analyzes situations in which the circumstance enhances hydrogen embrittlement, and it is divided into three main sections. Firstly, the effect of hydrogen on structural steels (pearlitic and austenitic) is revised, covering experimental, numerical and analytical aspects. Later, the study is extended to pearlitic steels with different degrees of cold drawing, on the basis of a materials science approach (relationship between microstructure and properties). Finally, a theoretical study is provided of the validity of the fracture mechanics approach to the phenomenon of hydrogen assisted cracking, analyzing the K -dominance condition to elucidate the role of the *far field* and the effect of *history*, the latter recalling the words of the Spanish poet Antonio Machado: "hoy es siempre todavía", and perhaps T. S. Eliot's "and all is always now".

Introduction

Paraphrasing the Spanish philosopher Ortega y Gasset, one could really say that *the material is itself and its circumstance*, which indicates, firstly, that the material is intrinsically imperfect, and therefore, that surface or internal defects are inherent in it; and secondly, that there is an evolution of its mechanical properties throughout the service life, due to the combined effect of the mechanical load history and the surrounding physico-chemical environment.

This consideration of the material as a live entity immersed in the surrounding environment has an important consequence: the concept of material is strongly linked with the existence of superficial or internal defects or geometrical flaws such as cracks or notches (from the macroscopical point of view) or imperfections in the microstructure such as lattice defects, dislocations, micro-voids, etc (from the microscopical point of view).

Thus the classical approach in mechanical and structural engineering in which the material is totally defined by its constitutive equation—or, even worse, merely by its elastic properties—turns to new approaches (materials science and fracture mechanics approaches) according to which material behaviour depends not only on the intrinsic characteristics of the material itself, but also on the circumstance, i.e., on extrinsic factors such as load history (load magnitude, kind of loading, loading rate, etc) and environment (temperature, humidity, corrosive agents, etc.) which make previous defects grow. It is important to notice, therefore, that a given material does not have a behaviour *per se*, but can exhibit one or another behaviour depending on the *circumstance*, i.e. on the specific working conditions (mechanical and physico-chemical environment). In this paper the hydrogen environment plays the role of circumstance.

Evaluation and modelling of hydrogen assisted fracture in structural steels

The hydrogen embrittlement phenomenon in structural steels is of fundamental importance in engineering, since hydrogen can be present in the material after the manufacturing process, or can enter it by electro-chemical reactions associated with stress corrosion cracking. The significance of hydrogen induced cracking is evident if one considers that hydrogen appears in a wide range of potentials, and that *local* electro-chemical conditions at a crack tip may differ substantially from those of the surrounding bulk environment.

In the last decades the study of embrittlement and/or degradation of metals and alloys in hydrogen has received a great deal of attention with the advance of fracture mechanics, which allows the formulation of models describing crack initiation and growth or the evolution of damage in hydrogen environments. The phenomenon has received many names more adequate for the new techniques and thus, apart from the traditional *hydrogen embrittlement*, other designations are used such as *hydrogen assisted cracking*, *hydrogen induced damage*, *hydrogen degradation*, *hydrogen assisted failure*, or one which is at the same time traditional and general: *hydrogen assisted fracture* (or *hydrogen induced fracture*) which seems to be the best to describe the complexity of the phenomenon in classical terms.

This section of the paper offers a generalized approach to the evaluation and modelling of hydrogen assisted fracture in two structural steels of special interest in engineering: a high-strength pearlitic eutectoid steel for civil engineering purposes (in the prestressed concrete technique) and an AISI type 316L austenitic stainless steel for fusion nuclear technology as a candidate material for the first wall of the next European fusion reactor (NET). The sub-sections are devoted to the micromechanical effects and the continuum mechanics approach, as well as to the kinematic, chemical and mechanical modelling of the damage/failure process.

Experimental evaluation of hydrogen assisted fracture in pearlitic steels.

Phenomenological study. Paper [1] presents a phenomenological study of the hydrogen embrittlement phenomenon in pearlitic steels, using pre-cracked and notched specimens subjected to slow strain rate testing (SSRT) in aqueous solution under hydrogen embrittlement environmental conditions produced by cathodic polarization during the test with potentiostatic control.

Test severity was measured through the ratio of the fracture load in solution to the fracture load in air (F_c/F_0). Fig. 1 shows the experimental results of the hydrogen embrittlement tests on pre-cracked samples. There are two regions of potential (E) leading to corrosion assisted failures. The lower region (that appearing in Fig. 1, associated with the most negative potentials) is called the cathodic regime, and the associated phenomenon is hydrogen assisted cracking (or hydrogen embrittlement), whereas the upper region (less negative potentials) is called the anodic regime, and the associated process is localized anodic dissolution (or pure stress corrosion cracking), although a hydrogen induced process could also appear.

The effect of the fatigue pre-cracking load consists in delaying either stress corrosion cracking or hydrogen embrittlement (Fig. 1), i.e., the higher the maximum stress intensity factor (SIF) during the last stage of fatigue precracking (K_{max}), the higher the fracture load under aggressive environment. This demonstrates the important role of residual stresses in environmentally assisted cracking; these residual stresses, of compressive type, are generated in the vicinity of the crack tip during fatigue pre-cracking of the samples.

In the case of localized anodic dissolution, residual stresses modify the local strain at the crack tip, thus changing the balance between the creation and rupture of oxide film. On the other hand, in hydrogen assisted cracking phenomena, compressive residual stresses delay both the hydrogen ingress and the hydrogen transport by diffusion driven by the hydrostatic stress field.

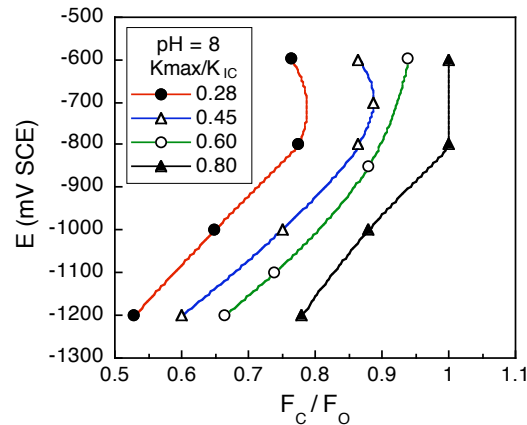


Fig. 1. Experimental results of hydrogen embrittlement tests (SSRT) on pre-cracked samples of high-strength pearlitic steel, for different values of the maximum stress intensity factor during the last stage of fatigue pre-cracking (K_{max}); K_{1c} is the fracture toughness.

Crack growth kinetics and meaning of thresholds

As part of the experimental research on the hydrogen embrittlement phenomenon, the crack growth kinetics (CGK) curve was also studied by means of constant strain tests (CST), with special emphasis on the meaning and evaluation of thresholds, which could lose their intrinsic character to depend on mechanical variables such as the maximum fatigue pre-cracking load [2], which demonstrates that the crack growth threshold in stress corrosion cracking (K_{ISCC}) depends dramatically on the fatigue pre-cracking SIF K_{max} .

These K_{max} -effects, due to compressive residual stresses in the vicinity of the crack tip generated during pre-cracking, were considered in the ISO 7539-6 Standard, which recommends that pre-cracking should be completed below the expected threshold K_{ISCC} , if possible. However, this requirement is not clearly objective, since the threshold does not have an intrinsic character, but is affected by the pre-cracking procedure itself. Furthermore, the requirement of the Standard could be automatically reached [3] because, in some material-environment systems, the maximum stress intensity factor K_{max} during the final stage of fatigue pre-cracking is *always* below the actual stress corrosion cracking threshold K_{ISCC} , as demonstrated in Fig. 2 for both hydrogen assisted cracking (HAC) and localized anodic dissolution (LAD).

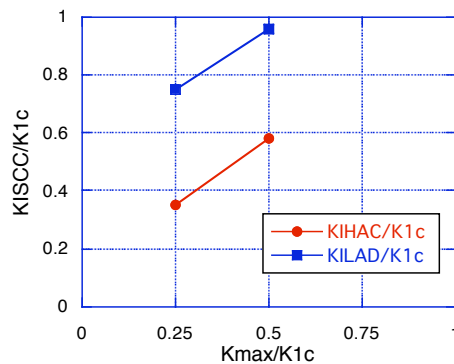


Fig. 2. Threshold in environmentally assisted cracking as a function of K_{max} (K_{IHAC} : for hydrogen assisted cracking, K_{ILAD} for localized anodic dissolution); K_{1c} is the critical SIF in air.

Fractographic analysis:tearing topography surface

Fractographic analysis of samples tested in the cathodic regime (i.e., in hydrogen embrittlement environmental conditions) always showed the same general aspect [4]: fracture initiates at an edge region in the vicinity of the crack or notch tip where the microscopic fracture mode may be classified as *tearing topography surface* or TTS.

Such a topography is a non-conventional microscopic mode of fracture, different from the four traditional micro-fracture modes: intergranular, cleavage, quasi-cleavage and micro-void coalescence (or fibrous, or dimpled) fractures. The tearing topography surface consists of micro-damage due to the hydrogen, in a kind of really complex and closely spaced nucleation of very small micro-voids at the micro-scale.

The TTS zone appears only under cathodic potentials ($E=-1200$ mV vs. SCE). It is not only a fracture mode, but also a propagation mode associated with sub-critical cracking, the crack growth rate being clearly lower than that of the cleavage topography. The tearing topography surface thus represents the *process zone* or *damaged area* (from the phenomenological point of view), and the *critical domain* or *fracture region* (from the fracture mechanics point of view).

Continuum mechanics approach to hydrogen assisted fracture of pearlitic steels

Macroscopic variables governing the microscopic fracture

The main objective of continuum mechanics analysis is to obtain the macroscopic internal variables (stress, strain, strain energy density,...) at the fracture instant. Since the outcome of a fracture test in inert or aggressive environment consists of external variables (load and displacement), it is necessary to relate the internal and external variables. The computational method used to this end was the finite element method with an elastic-plastic code.

The elastic-plastic finite-element analysis of notched geometries demonstrated that the hydrostatic stress distribution is practically invariable throughout the loading process in the matter of relative values, so that, in spite of the generally increasing stress level, the point of maximum hydrostatic stress remains at a constant depth x_s from the notch tip, a distance which is a characteristic of the geometry [5].

With regard to the relationship between the macroscopic internal variables (in the continuum mechanics sense) and the TTS microscopic mode of fracture, Fig. 3 shows that the TTS depth increases with the time to failure in SSRT with notched specimens, and there is an asymptotic value of TTS depth (x_{TTS}) in quasi-static tests (slow enough to allow the hydrogen equilibrium concentration to be reached). Results of the numerical analysis showed that such an asymptotic value $x_{TTS,\infty}$ is equal to x_s , the depth of the maximum hydrostatic stress point of the given geometry.

TTS zone and hydrogen embrittlement

The TTS area is not due to hydrogen alone but requires the combined action of stress-strain fields, so that the fracture takes place when a critical combination of hydrogen concentration and stress (or strain) is achieved. However, there is clear experimental evidence of the association between the TTS and the presence of hydrogen. The experimental results supporting this assumption are given in the following paragraphs:

- The microscopic appearance of the TTS resembles micro-damage, micro-cracking or micro-tearing due to hydrogen degradation, the scale of micro-damage being probably below $1\ \mu\text{m}$. [4].
- The TTS micro-fracture mode is a slow (or subcritical) crack growth topography associated with the stage II or *plateau* in the crack growth kinetics curve [4], i.e., with a constant crack growth rate independent of SIF.

- The TTS micro-fracture mode appears *only* under cathodic potentials (i.e. in hydrogen environment), but not under anodic ones, thereby providing fractographic evidence of hydrogen effects [4].
- The TTS size increases when the electro-chemical potential becomes more cathodic or negative. This is a consequence of the higher amount of hydrogen at the specimen surface for the more cathodic potentials [1].
- The TTS size slightly increases as the pH decreases (becomes more acid), since the amount of hydrogen supplied to the sample is higher in the case of lower values of the pH [1].
- The TTS size clearly decreases as the fatigue load increases. The reason for this is the presence of compressive residual stresses near the crack tip, induced during fatigue precracking [1].
- Experiments conducted at very different strain rates also showed an increasing trend of the TTS size as the time to failure increases, a consequence of a mechanism of transport based on stress-assisted hydrogen diffusion and time derivatives [6].
- The TTS size is clearly influenced by the geometry of the sample, through the hydrostatic stress distribution in its vicinity, which is also consistent with an association between the TTS failure mode and the hydrogen diffusion transport mechanism [6].
- The asymptotic TTS depth for quasi-static tests (slow enough to allow the hydrogen equilibrium concentration to be achieved) reaches the maximum hydrostatic stress point in the specimen, which confirms that hydrogen diffuses towards that point [6].

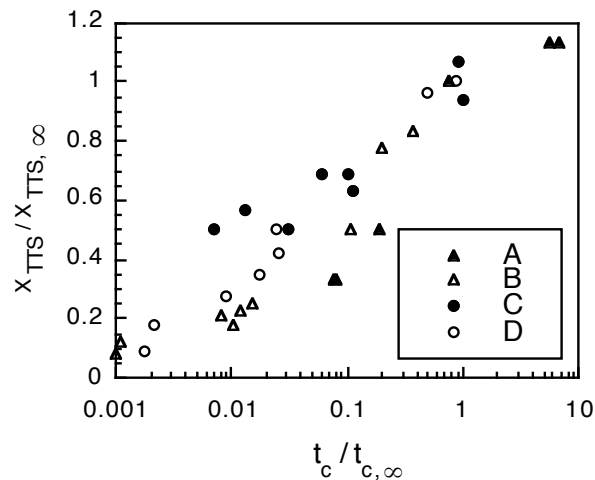


Fig. 3. Relationship between the TTS depth (x_{TTS}) and the time to failure (t_c) in notched samples A, B, C and D. Variables are divided by their respective values in the quasi-static test of each geometry ($x_{TTS,\infty}$ and $t_{c,\infty}$).

From the fracture mechanics viewpoint, the TTS topography is associated with a *transition (or critical) SIF* in the crack growth kinetics curve ($da/dt-K$) at which the crack growth rate progresses from the subcritical to the critical regime and the microscopic mode of fracture changes from the subcritical TTS mode to the cleavage (unstable) critical propagation [7], which allows a consideration of the progressive spreading of the TTS zone as a macroscopic crack extending the original fatigue pre-crack within the framework of linear elastic fracture mechanics. The critical SIF in hydrogen environment depends on fundamental testing variables closely related to hydrogen transport, such as the electro-chemical potential (increasing function), the fatigue pre-cracking SIF (increasing function) and the TTS depth itself (decreasing function), cf. [7].

In addition, further research [8] showed a kind of orientation in the TTS topography which evolves from oriented TTS to non oriented TTS and finally quasi-MVC (micro-void coalescence)

topography. Thus the latter could be considered as a candidate to TTS in which hydrogen could enhance void growth. When a greater amount of hydrogen reaches the material, the strongly hydrogenated areas turn from MVC to TTS, and this final phase of growth or link-up could be further influenced by hydrogen. The mechanism of hydrogen-enhanced void growth is different to that in air which consists of triaxiality-induced void growth, cf. [8].

Hydrogen transport: diffusion vs. dislocation movement

Hydrogen embrittlement of metals and alloys is a general phenomenon of degradation of mechanical properties which involves hydrogen transport to the prospective fracture locations, and there seems to be general agreement that hydrogen transport plays a dominant role in hydrogen assisted fracture. The question of the main hydrogen transport mechanism being operative over long penetration distances is still open, and two basic transport modes have been proposed to explain the phenomenon: *diffusion* (also called lattice diffusion, random-walk diffusion or \sqrt{Dt} diffusion), and *dislocation sweeping* (or dislocation dragging). A key point is to determine whether the main part of *macroscopic* hydrogen transport—that resulting in embrittlement with *detectable* loss of mechanical properties—is carried out by lattice diffusion or by dislocation movement, the latter associated with interactions between hydrogen and plasticity.

Diffusion is a transport mode by which hydrogen moves towards the points of minimum concentration through the crystalline lattice in the form of random-walk governed by the \sqrt{Dt} term which controls the penetration distance. If stress-assisted diffusion is considered, hydrogen movement is driven by the gradients of both concentration and hydrostatic stress. In the case of a formulation on the basis of stress- and strain-assisted diffusion, the plastic strain magnitude should be considered as one of the governing factors of hydrogen diffusion. A mechanism of hydrogen transport based on lattice diffusion is consistent with the results of slow strain rate tests under cathodic polarization environmental conditions, since it predicts maximum embrittlement at the slowest strain rates. On the other hand, diffusion is usually a slow transport mode and penetration distances are rather small.

Dislocation sweeping is a transport mode by which hydrogen is dragged by dislocations as the plastic zone spreads. This process may be associated with the average velocity of dislocations which can be macroscopically expressed in terms of the plastic strain rate. There are two main models to evaluate the supersaturation or enrichment of hydrogen at specific sites in the material as a result of a dislocation sweep-in of hydrogen: the *stripping model* by Tien *et al.* and the *annihilation model* by Johnson and Hirth, cf. [9]. The first model estimates a significant build-up of hydrogen, while the latter concludes that the kinetic supersaturations are extremely small in all real situations. The weakest point of the two models is their inconsistency with the well known experimental evidence of the inverse dependence of hydrogen embrittlement upon strain rate (over a really wide range of strain rates between the two limit situations). The stripping model predicts maximum hydrogen embrittlement at an intermediate strain rate, whereas according to the annihilation model the kinetic supersaturation is proportional to the strain rate.

The two transport modes (diffusional and dislocational) are essentially different. The first one is operative under both sustained and transient (time-dependent) stress-strain states, has hydrostatic stress and *instantaneous* plastic strain as responsible variables, and evolves towards equilibrium hydrogen distributions. In contrast, the other mode proceeds exclusively during continuing (dynamic) straining, has plastic strain *rate* as the governing variable, and results in non-equilibrium hydrogen distributions (temporal local over-saturations). They are fed by newly arriving dislocations which drive hydrogen into specific microstructural sites, from which hydrogen escapes by diffusion to restore thermodynamic equilibrium with local surroundings. After the end of straining, those

hydrogen over-saturations relax to local equilibrium by *short-range* (local) diffusion. The efficiency of this mode of hydrogen transport results from competition between these two effects.

Thus the role of hydrogen transport by dislocation dragging is strongly linked with hydrogen-plasticity interactions in the steel. The relationship between hydrogen and plasticity is a fundamental topic which has been the object of many controversial discussions in two opposite senses: whether or not hydrogen influences plasticity development by promoting slip bands or strain localization, and conversely, whether or not plastic zone development—and subsequent movement of dislocations—can affect hydrogen transport. Thus a key question arises: whether or not dislocation transport can be considered an embrittlement mechanism *per se* with *detectable* loss of mechanical properties as a consequence of macroscopic hydrogen transport.

As described in [9], the concept of symmetry of the Onsager coefficients could be applied to hydrogen transport by mobile dislocations, thus considering the coupled problem of hydrogen-dislocations interactions [$H \leftrightarrow \perp$] in the double sense: (i) hydrogen transport by dislocations or dislocational transport of hydrogen [$\perp \rightarrow H$]; (ii) dislocation transport by hydrogen or hydrogen-enhanced strain localization [$H \rightarrow \perp$].

Therefore, since dislocations are able to carry hydrogen, the presence of hydrogen is able to promote dislocation movement in the form of localized slip bands and strain localization. From the macroscopic point of view, it seems feasible that to the extent that hydrogen does not affect the macroscopic constitutive equation of the metal, the transport of hydrogen by dislocation sweeping should not have a macroscopic effect.

Experimental evidence of hydrogen transport by stress-assisted lattice diffusion in pearlitic steel was provided in [9] by means of a fractographic analysis of the region microscopically affected by the hydrogen (*the tearing topography surface TTS*) and a numerical study of the evolution of the zone of dislocation movement (*the plastic zone PZ*), which showed that in some cases the hydrogen affected area clearly exceeds the only region where dislocations can move, which in turn seems to demonstrate that diffusion is the predominant mode of transport in pearlitic steel under triaxial stress states produced by notches. It is not, however, conventional diffusion according to Fick's laws, but stress-assisted diffusion in which the hydrostatic stress field plays a very important role, by increasing the concentration at the boundary and by enhancing hydrogen flux associated with stress gradients.

It is significant that the depth of the TTS region in such quasi-static tests reaches the point of maximum hydrostatic stress, as mentioned in previous sections. Hydrostatic stress at the boundary controls the fracture process in quasi-instantaneous tests, since diffusion cannot take place in these tests due to their short duration [10]. In this case the environmental action is restricted to the notch tip. The triaxiality factor (defined as the maximum value of the stress triaxiality in the sample) governs the fracture process in quasi-static tests. In this case, the environmental effect depends on hydrogen diffusion towards the points of maximum hydrostatic stress [10].

These experimental findings are not consistent with dislocation transport of hydrogen, so, in spite of the fact that this specific mode of transport has been sufficiently demonstrated on a microscopic scale, it might not be a really critical step for hydrogen embrittlement on a macroscopic scale, detectable with loss of fracture load. Thus hydrogen transport by dislocation dragging is a well established phenomenon, but the question of whether or not it should be considered as a mechanism of embrittlement *per se* still remains open.

Lattice diffusion and dislocation sweeping may be predominant depending on the specific material and external conditions, so any hydrogen embrittlement theory should consider both transport modes. In this framework, and to rationalize hydrogen embrittlement data, it would be extremely important to discriminate the effects of hydrostatic stress fields from those of equivalent stress distributions (related to plastic zone progress) to evaluate the predominant mode of hydrogen

transport on a macroscopic (continuum mechanics) scale. The same applies to the discrimination between the two commonly competing effects associated with dislocation movement: enhanced transport and enhanced trapping of hydrogen.

Kinematic modelling of hydrogen assisted fracture of pearlitic steels: role of local strain rate

This section deals with a kinematic modelling (strain-rate based) of hydrogen induced fracture in round notched samples and pre-cracked specimens of high strength steel. It is well known that environmentally assisted fracture (EAF) phenomena are localized and transient, the effect of strain rate being relevant. However, when precracked or notched specimens are used, it is the local strain rate at the crack or notch tip—and not the externally applied testing displacement rate—that is the variable controlling the environmental process.

The present approach consists of the calculation—by analytical or numerical methods—of the local strain rate at a crack or notch tip as a function of the global strain rate in the specimen. *Local or effective strain rate* is the damage variable governing the EAF process, whereas *global, nominal or applied strain rate* is the control variable during the test.

In ref. [11], the approach was applied to the formulation of a kinematic fracture criterion for round notched samples of high strength steel under hydrogen embrittlement environmental conditions. Experimental results of hydrogen embrittlement tests, represented as a function of global strain rate, were seen to be dependent on the geometry. To unify the results, the average value of the equivalent stress was computed over the critical region or microscopically affected zone (TTS). In addition, local strain rate in the vicinity of the notch tip was averaged over the critical region (space average) and throughout the test duration (time average). The final operation was the change of variable from global to local strain rate. Fig. 4 gives the results according to this approach, showing that most of them fit into the same *universal curve* (geometry-independent). The limit of applicability of this formulation is given by the asymptotic value (for quasi-static tests) of the critical equivalent stress for each geometry, represented by the horizontal dashed lines in the left part of Fig. 4.

In ref. [12] a simple analytical procedure was proposed to estimate the local strain rate at a crack tip and again the estimation was experimentally checked by applying the kinematic fracture criterion proposed previously [11] for high strength steel under hydrogen embrittlement environmental conditions. Calculation of the local (crack tip) strain rate was performed on the basis of the elastic displacement distribution in the vicinity of a crack tip in conditions of plain strain, cf. [12]. The depth of the maximum hydrostatic stress point (the other relevant variable in hydrogen assisted cracking) was obtained by using approximate stress distributions in the vicinity of the crack tip in the elastic-plastic regime, or was calculated as the asymptotic depth (for quasi-static tests) of the hydrogen affected area. Fig. 5 shows the results of this approach in dimensionless form. If compared with Fig. 4, it is clear that both sets of experimental results show the same trend when expressed in terms of the dimensionless local strain rate in the vicinity of the crack or notch tip, which confirms the very important role of this variable in hydrogen embrittlement processes in the presence of stress or strain localization near a crack or notch.

Furthermore, on performing a linear fitting of the results of Fig. 4 (notched samples) and Fig. 5 (cracked samples), the following equations are obtained:

Notched samples:

$$\sigma^* = 0.15 \log \varepsilon^* + 0.99 \quad (\varepsilon^* \geq \varepsilon_{\infty}^*)$$

Cracked samples:

$$\sigma^* = 0.13 \log \varepsilon^* + 0.96 \quad (\varepsilon^* \geq \varepsilon_{\infty}^*)$$

which demonstrates that the two approaches produce an almost identical kinematic relationship between the dimensionless stress σ^* and the dimensionless strain ϵ^* .

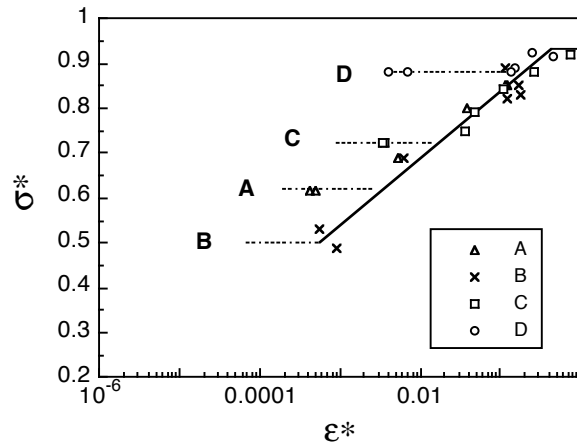


Fig. 4. Kinematic modelling of hydrogen assisted fracture of round notched samples: critical equivalent stress in hydrogen environment (σ^*) as a function of the average value of the *local* strain rate in the vicinity of the notch tip (ϵ^*); dimensionless variables, cf. [11]. Horizontal dashed lines refer to the quasi-static tests.

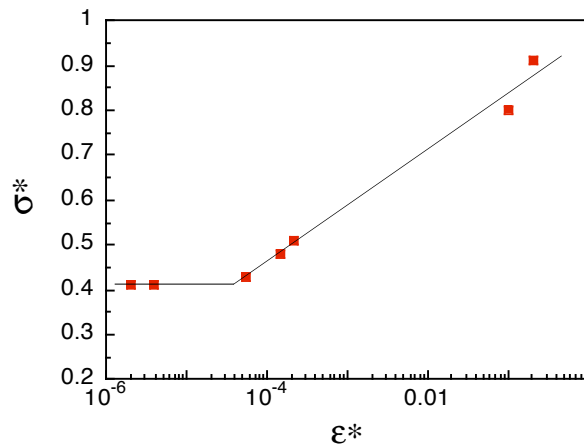


Fig. 5. Kinematic modelling of hydrogen assisted fracture of pre-cracked samples: critical equivalent stress in hydrogen environment (σ^*) as a function of the average value of the *local* strain rate in the vicinity of the crack tip (ϵ^*); dimensionless variables, cf. [12].

Paper [13] goes further in the analysis of notch-tip local strain rate and demonstrates that the relationship between local and global strain rates depends not only on the specimen geometry but also on the stress-strain curve of the material and on the load applied on the sample (the latter two factors controlling the plastic strain distribution in the overall geometry, and particularly in the vicinity of the notch tip), which implies that local strain rate changes with time, even for constant global strain rate externally applied, as in the case of slow strain rate tests. The spreading of the plastic zone is the key item to determine the evolution of the notch tip strain rate, which demonstrates the importance of the notch geometry and the constitutive equation of the material (stress-strain curve). This material dependence is also present in cracked geometries, and thus crack

tip strain rate depends also on the stress-strain relationship and changes with time, which indicates that further refining of available models and estimations is required.

In ref. [14], the local strain rate at a crack tip of a cracked cylindrical specimen was numerically computed as a function of the global strain rate externally applied (or testing displacement rate) for cracked geometries of different crack lengths and distinct constraint stress states (axisymmetric and plane strain). The global analysis demonstrated that the extension of the plastic zone is broader in the plane-strain specimens (higher equivalent stress), while the level of hydrostatic stress is higher in the axisymmetric specimens. The local strain rate at the crack tip changes as the straining proceeds, i.e., it depends on the global strain externally applied at the sample ends. In axisymmetric specimens, the crack-tip strain rate increases monotonously as the straining proceeds, whereas in the plane-strain specimens the relationship between local and global strain rate is almost constant when a certain level of straining is reached. The application of these results to stress corrosion testing is discussed in [14].

Chemical modelling of hydrogen diffusion in pearlitic steels: role of residual stresses

This section illustrates chemical modelling of environmentally assisted fracture processes, and describes a computer model to predict the life of prestressing steel wires in a standard solution that promotes hydrogen embrittlement. The model allows the introduction of residual stresses which influence the hydrogen concentration at the wire surface and the hydrogen diffusion towards the inner points, thus conditioning the life of the wire in the solution. It is based on the following hypotheses [15]:

• Hypotheses of diffusion

D1. Hypothesis of absorption.— The absorption of adsorbed hydrogen at the metal surface is considered quasi-instantaneous. Hydrogen embrittlement tests on brittle materials such as high-strength prestressing steels confirmed this assumption, since the damaging effect of hydrogen is detectable even in very short tests. The hypothesis was also verified in highly ductile metals such as austenitic stainless steels, so it is assumed to be valid for an extended set of materials with ductile or brittle behaviour in the presence of hydrogen.

D2. Hypothesis of transport.— It is assumed that the main hydrogen transport mechanism is stress-assisted diffusion. This hypothesis was seen to be adequate for high-strength steels in aqueous environments promoting hydrogen embrittlement, and even for austenitic steels with a modified hydrogen diffusion coefficient in the damaged material. The other important mechanism of hydrogen transport (dislocation movement) is not very important in specimens under quasi-static loading. An effective diffusion coefficient is considered to account for the hydrogen traps (static dislocations and others).

D3. Hypothesis of cylindrical symmetry.— The hydrogen entry and diffusion towards the inner points are assumed to possess cylindrical symmetry, i.e., every point of a circumference with its centre at the cylinder axis is supposed to receive the same amount of hydrogen, the concentration depending only on the radial length (distance from the free surface). This hypothesis is consistent with the specific symmetrical character of the process itself, so it is assumed that there is no difference between points located at the circumferences, i.e., no privileged points for diffusion are allowed.

• Hypotheses of fracture

F1. Hypothesis of damage localization.— The fracture phenomenon is spatially localized and the damage is assumed to be concentrated as a discrete part-through crack perpendicular to the bar axis, thus losing the cylindrical symmetry. Then, although hydrogen diffusion is considered to be axisymmetric (and thus hydrogen concentration is constant along circumferences) there is a certain

time at which local damage in the form of a crack appears, in the same way as the necking phenomenon emerges in a standard tension test. This hypothesis seems to be more adequate for high-strength steels (brittle) in which damage localization appears as a discrete surface crack, whereas in austenitic stainless steels (ductile), hydrogen damage develops continuously in volume in the form of notch extension.

F2. Hypothesis of initiation.— Fracture initiates when the hydrogen reaches a critical concentration c_c over a distance x_c (process zone, damaged area or critical size for initiation); then it is assumed that a crack of depth x_c is created and that this is precisely the *embrittled zone*. The critical concentration c_c depends on the environmental conditions (hydrogen embrittlement in this case) and thus is considered as a material property.

F3. Hypothesis of propagation.— The propagation time, i.e., the time required to propagate the crack from the initial size x_c up to a critical value to produce the final fracture of the sample, is neglected. Then it is assumed that the initiation time coincides with the time to fracture or critical time t_c . In accordance with this hypothesis, the damage process is time-localized just at the instants previous to the global catastrophic failure of the structural element, which is feasible in high-strength steels considering the rather high sub-critical crack growth rate. In austenitic steels the hypothesis also seems adequate, since the effects of hydrogen can only be detected in the final stages of fracture unless very high fugacities of hydrogen are used.

With *F1* the fracture phenomenon is modelled as a damage process spatially localized, whereas *F2* and *F3* imply a time localization of damage/fracture. Although the initiation of fracture is really a progressive process, it is assumed that the specimen remains unaffected until a crack of depth x_c is created (space localization), the moment at which it propagates in an unstable manner up to the final fracture (time localization). This implies that initiation and fracture criteria are equivalent and that there is no subcritical crack growth.

The model was experimentally checked in [16] by performing numerical computations on steel wires with very different residual stress profiles and comparing model predictions and experimental results of the Ammonium Thiocyanate Test (ATT) proposed by the International Federation for Prestressing (FIP) to evaluate the susceptibility to hydrogen embrittlement of prestressing steels. The computational results—in the form of curves of the applied stress vs. time to failure—for the material with zero, tensile and compressive residual stresses, are shown in Figs. 6 (35°C) and 7 (50°C), together with the boundaries of the experimental scatter band (dashed lines). In both cases the agreement between model predictions and experimental results is excellent, because the curve for the material free of residual stresses exactly fits the central tendency of the experimental results, whereas curves for tensile and compressive residual stresses approach the boundaries of the experimental scatter area, which demonstrates the goodness of the proposed approach—and its computer model implementation—to estimate the wire life in the ATT and thus to analyze the role of surface residual stresses in the hydrogen embrittlement susceptibility of prestressing steel wires.

Tensile residual stresses enhance hydrogen penetration into the critical area, thus decreasing the life of the wire, whereas compressive residual stresses delay the hydrogen ingress, thus extending the wire life. The explanation of these assertions lies in the fact that hydrogen diffusion is governed not only by the concentration gradient, but also by the hydrostatic stress field in the material which is itself influenced by the residual stress distribution. This also explains why the experimental scatter increases as the externally applied stress decreases and the residual stress level becomes more important.

Paper [17] emphasizes the important effects of residual stress levels on hydrogen embrittlement susceptibility of prestressing steels, since the steel wire behaves *as if* the stress level effectively acting on the damage process were the real applied stress plus the main level of residual stress (average value). Therefore, an *effective stress* may be defined as $\sigma_{\text{eff}} = \sigma_{\text{app}} + \sigma_{\text{res}}$, where σ_{app} is the

stress externally applied in the ATT test and σ_{res} the average residual stress level. In Fig. 8 a plot is given of the above defined effective stress as a function of the time to failure. At both temperatures, the results associated with the different levels of residual stresses fit into the same curve, which indicates that the time to failure in the ATT is a single function of the effective stress and this is the relevant variable in engineering design against hydrogen assisted cracking (or hydrogen embrittlement) of prestressing steel wires.

The concept of effective stress is a useful tool in design of prestressed concrete structures. It indicates that variations of residual stress and increments of externally-applied stress are equivalent from the point of view of hydrogen embrittlement. Thus the engineer can choose the best prestressing steel on the basis of the residual stress distribution induced by the manufacturing process (which can be measured by X-ray diffraction).

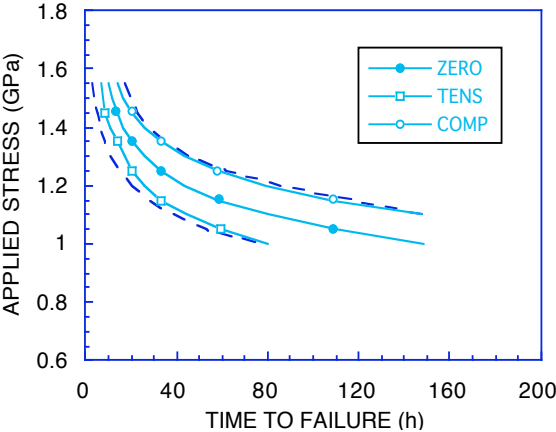


Fig. 6. Computational results at 35°C for different residual stress levels and boundaries of the experimental scatter area (dashed lines).

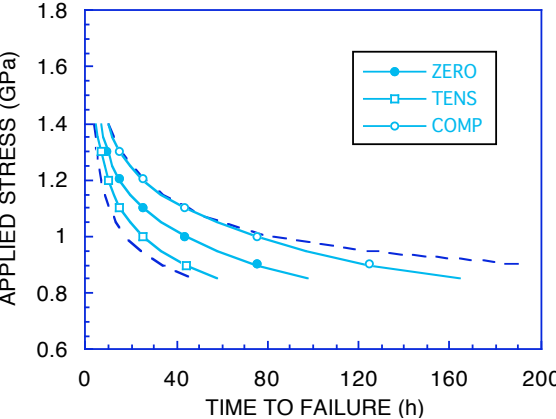


Fig. 7. Computational results at 50°C for different residual stress levels and boundaries of the experimental scatter area (dashed lines).

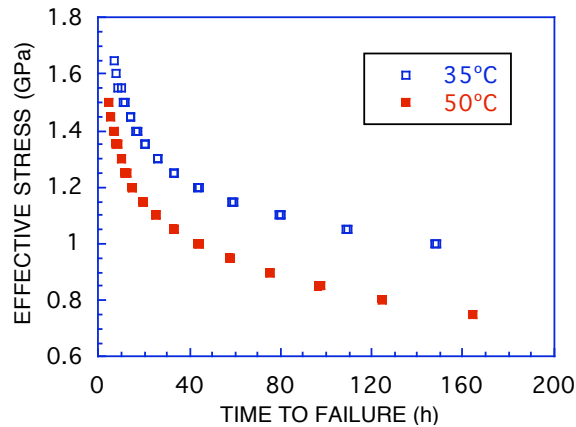


Fig. 8. Effective stress vs. time to failure

Mechanical modelling of hydrogen induced damage in austenitic steels: notch extension effect

In this section, two mechanical models are presented to describe the failure behaviour of 316L austenitic stainless steel notched bars in hydrogen. Tests [18] showed that macroscopic effects of hydrogen consisted of a decrease in fracture load almost independently of notch radius (for the same notch depth).

From the micromechanical point of view, hydrogen induced damage consisted of micro-cracking in the area surrounding the notch [19, 20], thereby suggesting two mechanical models to describe the embrittlement effect due to the presence of hydrogen [19, 20]. The *notch extension model* (NEM) considers that the hydrogen effect can be modelled as a geometric enlargement of the notch. In the *notch cracking model* (NCM), it is assumed that the embrittled area at the notch tip behaves as a macroscopic crack extending the original notch.

The two models are sketched in Fig. 9. In both, the failure load was calculated as a function of damage depth (c), where the latter means notch depth increment in the NEM and extra-crack depth in the NCM. The values for the NEM can be estimated by dimensional analysis, which gives the plastic-instability failure load for an axisymmetric notched bar, cf. [20]. Values for the NCM can be numerically computed by the finite element method with an elastic-plastic code. Then the load-elongation curves of notched specimens with cracks of different depths emanating from the notch tip were numerically obtained to determine the failure load corresponding to each crack length, as described in [20].

Hydrogen embrittlement test results for the two notched geometries used in the experimental programme (sharp notch specimen and blunt notch specimen) were given in terms of failure load decrease in hydrogen vs. embrittlement time (time to failure, up to the maximum load). Since model predictions were in the form of failure load decrease vs. damage depth, a data-fitting technique was used to obtain an evolution law of damage depth with time.

Fig. 10 shows model predictions and experimental results. By choosing the adequate time scale (second vertical axis) the experimental points cluster round the curve of the NEM. It is not possible to fit such results into the curve of the NCM, even changing the scales of the second y-axis. For the NEM, it might be possible to obtain a similar clustering by assuming a different evolution law for damage depth in time and some kind of relationship between this variable and the ratio a/R . This new damage NEM would be equivalent to the old one, but more complicated, in representing the

hydrogen effect from a mechanical viewpoint. Only a microscopical analysis of the shape and the evolution of the damaged zone would determine which is nearer to the physical reality.

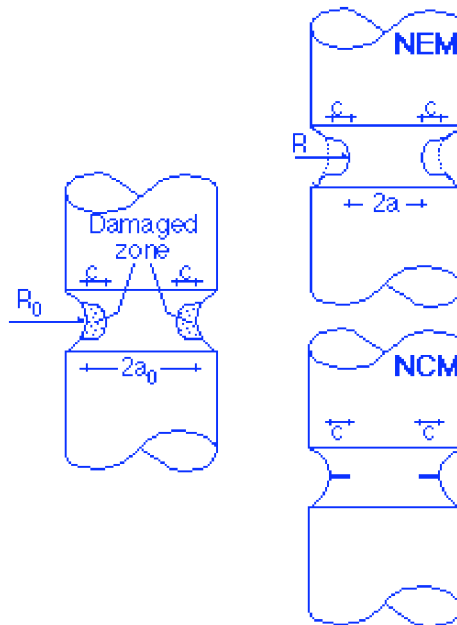


Fig. 9. Mechanical modelling of hydrogen induced damage in round notched specimens of 316L austenitic stainless steel: notch extension model (NEM) and notch cracking model (NCM).

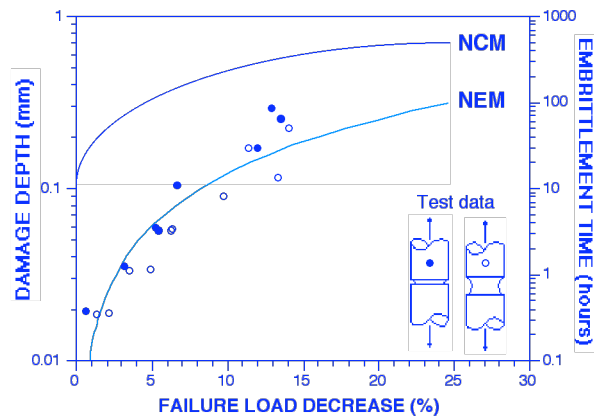


Fig. 10. Mechanical modelling of hydrogen induced damage in round notched specimens of 316L austenitic stainless steel: model predictions and experimental results.

Paper [21] goes further in the fractographic analysis of the broken specimens by assembling microfracture maps (MFM) of the whole fracture surface obtained by scanning electron microscopy (SEM), showing that the microscopical appearance of the *embrittled zone or area damaged by hydrogen* (external circumferential ring) is very rough and irregular at the microscale, with evidence of *microcracking* or *secondary cracking*, in contrast with the smooth surface (at the microscale) created by microvoid coalescence (MVC or *dimpled fracture*) in the inner core which is not embrittled by hydrogen.

The influence of the notch geometry on the MFM obtained in air is observed in the type of microvoids which appear in the MVC fracture surface. While in the sharp notched samples (higher triaxiality) the microvoid density is very high, the blunt notched samples (lower triaxiality) present lower microvoid density, although the maximum microvoid size is higher. This fact is consistent

with the classical models of void growth which assume that the triaxiality level enhances the void growth rate but limits the critical void size.

Hydrogen inhibits the void growth in the external ring and produces the microcracked topography. As a consequence, the triaxiality level in the internal core increases due to secondary cracking in the external ring, thus increasing the microvoid growth rate and lowering their critical size, so that the MVC appearance in the hydrogen embrittlement tests is similar in both notched geometries (after secondary cracking they reach a similar triaxiality level) and similar to that obtained in air for the sharp notched specimens.

With regard to the *embrittled zone* in the form of a microcracked ring, its appearance is similar in all tests, although its roughness increases as the embrittlement time increases, so that in the slowest tests the evidence of multi-cracking at different levels (and thus extended in volume) is clearer. The depth x of this embrittled zone was measured in the MFM in relation to the notch tip, and a plot representing this depth vs. the embrittlement time is given in Fig. 11, where it is observed that the damage depth increases with the test time. The results are not strongly dependent on the notch geometry, which is consistent with the previous reasoning, since the hydrogen damage consists of microcracking in the ring and this increases the triaxiality level and makes the behaviour of both notched specimens similar. In spite of this general trend, results for the sharp notched geometries seem to be above those for the blunt notched geometries, which could indicate that the stress—or strain—concentration enhances the hydrogen transport.

In [22], an integrated approach to the modelling of hydrogen assisted failure in 316L steel is presented. The approach includes experimental, fractographic, numerical and theoretical analysis. The physical adequacy of the mechanical models of hydrogen embrittlement (NEM and NCM) is discussed by comparing the *virtual damage depth* (theoretical) predicted by the models with the *embrittled zone* (micro-physical) measured in the fractographic analysis by scanning electron microscopy. To this end, Fig. 12 shows the comparison between model predictions and experimental results expressed as a relationship between damage depth measured by fractographic methods [21] and failure load in hydrogen environment. It is seen that the experimental results cluster round the curve of the NCM, which is more adequate from the fractographic viewpoint. It is thus demonstrated that the hydrogen damaged region (microcracked ring) may be modelled as a macroscopic crack extending the original notch. Thus hydrogen promotes surface microcracking (or secondary cracking) up to the point of maximum load (instability point) from which failure takes place by plastic instability associated with a microscopical mechanism of MVC.

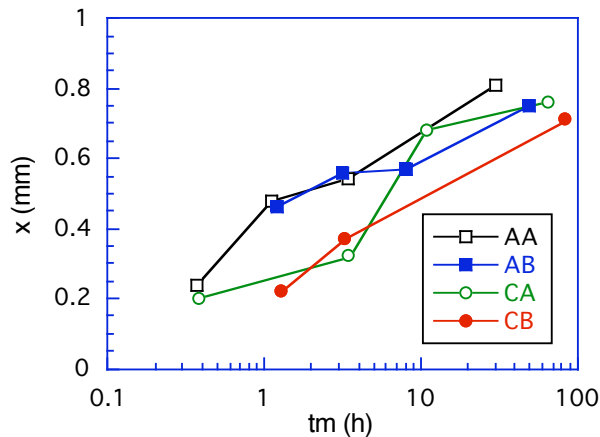


Fig. 11. Depth of the zone damaged by hydrogen as a function of embrittlement time.

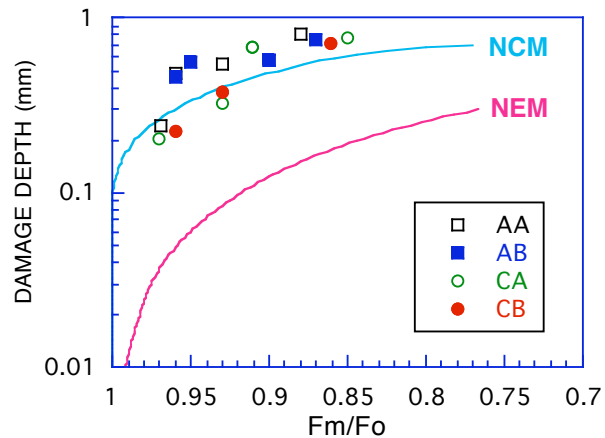


Fig. 12. Fractographic (microscopic) assessment of the models: comparison between model predictions and experimental results expressed as a relationship between damage depth and failure load F_m in hydrogen environment (F_o is the failure load in air).

Corrosion assisted cracking of progressively drawn pearlitic steel for civil engineering use: a materials science approach.

The study of high-strength prestressing steels is of special importance in civil engineering structures where prestressed concrete is widely used. These steels are manufactured from a previously hot rolled bar with pearlitic microstructure which is heavily cold drawn in several passes to produce the commercial prestressing steel wire with increased yield strength obtained by a strain-hardening mechanism. Thus the final commercial product has undergone strong plastic deformations able to modify drastically its microstructure.

Cold drawing induces progressive anisotropy in the material as a consequence of the important changes at the microstructural level. Although it is clear that cold drawing improves the (traditional) mechanical properties of the steel (i.e., those properties useful for regular engineering service), the microstructural changes during manufacture may produce anisotropic properties related to fracture and stress corrosion cracking and these effects could be dangerous when the materials work in aggressive environments. Thus, contributions to a better understanding of microstructural evolution in pearlitic steels subjected to cold drawing should be welcome, not only for purely scientific reasons, but also from the engineering point of view.

This section of the present review paper summarizes the achievements of a basic research line in the field of environmentally assisted cracking in general and of hydrogen degradation in particular. It deals with a materials science approach to the study of corrosion assisted cracking of progressively drawn pearlitic steels for civil engineering use. The approach is based on the fundamental idea of materials science: that of linking the microstructure of the different steels (progressively oriented as a consequence of the manufacture process by cold drawing) with their macroscopic stress-corrosion behaviour (increasingly anisotropic as the degree of cold drawing increases).

The first part of the research was the metallographic analysis. Attention was paid to the evolution with cold drawing of the two basic microstructural levels: the pearlite colonies (first level) and the pearlitic lamellae (second level). With regard to the first microstructural level, a progressive elongation and orientation of the pearlitic colonies in the cold drawing direction (wire axis) was observed. In the matter of the second microstructural level, the analysis showed an increasing closeness of packing (with decrease of the interlamellar spacing) and a progressive orientation of the pearlitic lamellar microstructure in the cold drawing direction. Therefore, both pearlite colonies and

pearlitic lamellar microstructure tend to align to a direction quasi-parallel to the wire axis as cold drawing proceeds.

The second part of the research consisted of a programme of stress corrosion cracking tests under both cathodic and anodic conditions to promote two very different mechanisms of cracking: hydrogen assisted cracking (HAC) and localized anodic dissolution (LAD). Both types of stress corrosion test confirm that the cold drawn steels exhibit anisotropic behaviour associated with a clear change in crack propagation direction which approaches the wire axis or cold drawing direction. In both regimes (HAC and LAD) there is a correlation between the microstructural orientation angles (at the two levels of pearlitic colonies and lamellae) and the propagation angles of the macroscopic crack, which clearly demonstrates the influence of the oriented microstructure — and thus of the manufacture process by increasing cold drawing— on the macroscopic corrosion-assisted behaviour of the steel wires.

Microstructural evolution with cold drawing

To analyze the progressive microstructural changes in the steel, samples from an industrial manufacturing process were used. The steel passes through several dies that produce a reduction of the wire section in each pass, and thus each stage can be characterized by its diameter. To perform this work, the manufacture chain was stopped in the course of the process, and samples of five intermediate stages were extracted, apart from the original material or base product (hot rolled bar not cold drawn at all) and the commercial product (prestressing steel wire heavily cold drawn). The metallographic analysis dealt with the two basic microstructural levels in pearlitic steels: the pearlite colony (i.e., the first microstructural level) and the pearlitic lamellar microstructure consisting of alternating plates of ferrite/cementite (second microstructural level).

Pearlite colony.- Longitudinal (L) and transverse (T) sections of all steels were cut and mounted to reveal the microstructure. The shape of the pearlite colony (i.e., the set of parallel ferrite and cementite lamellae) was modelled as an ellipsoid, as shown in Fig. 13. Thus the ellipsoidal axes allow a quantification of both the colony size and the orientation angle of the pearlite colony in relation to the main directions of the steel wire. In the L-section, the orientation angle β is measured between the wire axis (z direction) and a test line defined by the major axis (2c) of the elliptic section of the colony. In the T-section, the orientation angle θ is measured between the radial axis (r direction) and a test line defined by the major axis (2b) of the elliptic section.

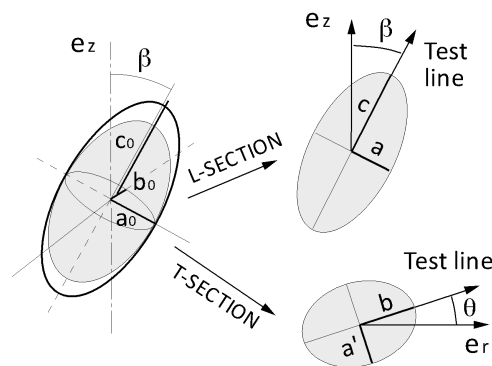


Fig. 13. Ellipsoidal model for the pearlite colony and procedure for measuring the orientation angles β (L-section) and θ (T-section).

In the matter of the size of the pearlite colonies [23], Fig. 14 plots the dimensions of the ellipsoid (L- and T-sections) as a function of the cold drawing degree represented by the ratio of the diameter of the steel wire at each stage of the process (D_i) to the initial diameter of the base material (D_0). In the L-section, the major axis length (2c; cf. Fig. 13) grows moderately until the fourth stage of cold drawing. From this stage, the effect of plastic deformation produced by cold drawing results in a marked enlargement of the main dimension of the pearlite colony. On the other hand, the minor axis 2a shows a slight decreasing trend and thus the difference between the axes 2a and 2c becomes larger as the cold drawn level increases. In the T-section, both major and minor axes (2a' and 2b) are shortened by the plastic deformation generated by drawing. The numerical values of the minor axes of the elliptical L- and T-sections (2a and 2a') are really similar, which indicates that the colony can be considered as axisymmetric, the axis of symmetry being that corresponding to the dimension 2c. With regard to the orientation of the pearlite colonies [24], Fig. 15 shows the evolution of the orientation angles for different degrees of cold drawing. In the L-section the angle decreases clearly with cold drawing while in the T-section it remains quasi-constant with a value near 50° , i.e., whereas a marked orientation effect in the cold drawing (axial) direction is detected in the L-cut (specially in the heavily drawn steels), a random orientation is found in the T-cut for all the drawing steps. It indicates that the colonies evolve towards an oriented arrangement.

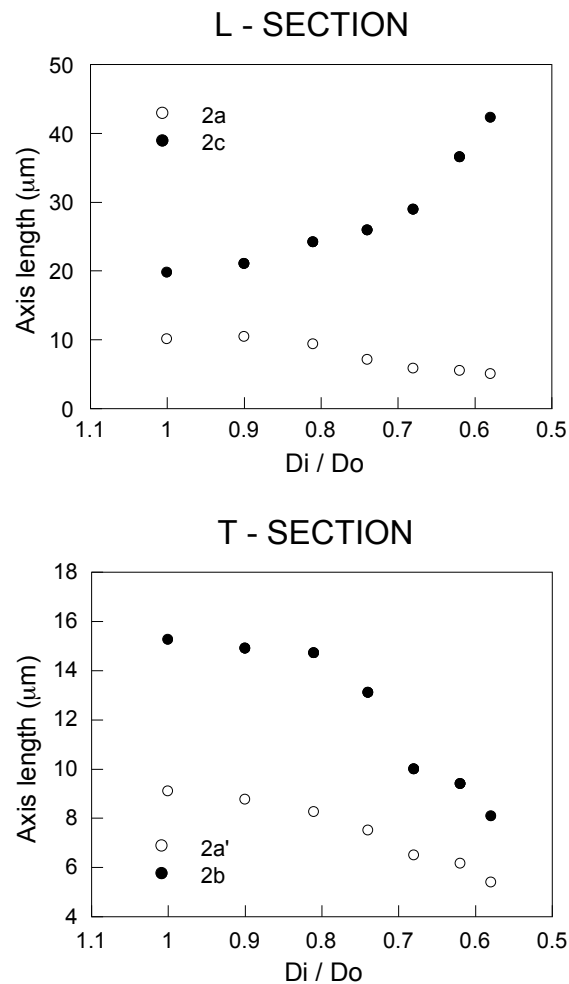


Fig. 14. Dimensions of the pearlite colony (L- and T-sections) for different degrees of cold drawing.

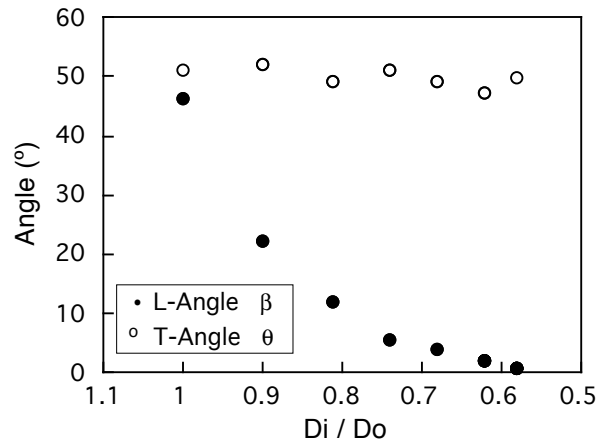


Fig. 15. Orientation angles β and θ (cf. Fig. 13) of the pearlite colony for different drawing degrees.

As a summary of the effects of cold drawing on the evolution of the pearlite colony, it can be said that a first effect of cold drawing is a progressive orientation of the pearlite colony with its main axis approaching the axis of the wire or cold drawing direction. This effect seems to be really predominant in the first stages of the manufacturing route.

The second effect of cold drawing is to slenderise the pearlite colony, producing a clear enlargement of the main axis (quasi-parallel to that of the wire) and a shortening of the secondary axis (perpendicular to the former). This effect seems to predominate in the final stages of the manufacturing route.

Pearlitic lamellar microstructure.- Scanning electron microscopy (SEM) was needed to resolve the lamellar microstructure of the pearlite. Fig. 16 offers the pearlite interlamellar spacing as a function of the degree of cold drawing [25]. During the drawing process, the ratio S_i/S_0 of the interlamellar spacing in an intermediate (i) step of the process to the initial (0) interlamellar spacing in the hot rolled base material decreases as the wire diameter diminishes, i.e., as the cold drawing proceeds.

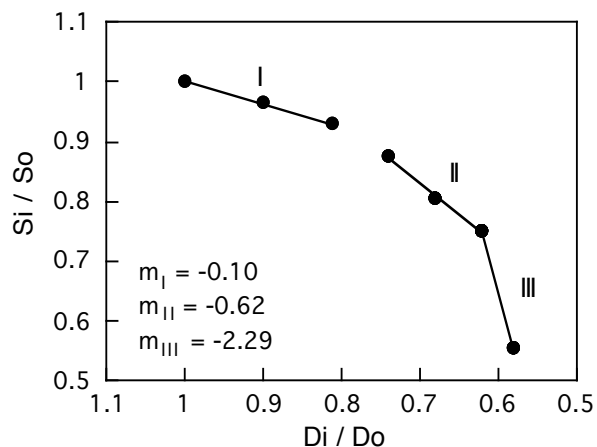


Fig. 16. Pearlite interlamellar spacing for different degrees of cold drawing.

This trend is maintained throughout the straining sequence, although the decrease rate of interlamellar spacing is not constant, so that three stages may be distinguished (cf. Fig. 16). Part I corresponds to slightly drawn steels for which the decrease of S_i is not drastic, and is reflected in the curve which shows a slight slope. In the second part (II) the slope is now significant. Finally the last part III which corresponds to heavily drawn steels has a very high slope which indicates that the decreasing rate of the interlamellar spacing is much higher than in previous phases of the process.

In the matter of the orientation of the pearlitic lamellar microstructure [26], Fig. 17 shows the ϕ angle between the radial direction of the wire and the vector normal to the cementite plates, measured in both L- and T-sections. Thus the angle ϕ in the L-section is 90° when the plates are aligned perpendicularly to the axial direction, and 0° when the plates are parallel to the axial direction. In the T-sections the angle exhibits no relevant difference between the steels. The L-section, on the other hand, shows a decreasing trend throughout the process, more intense in the later stages of the cold drawing (manufacturing) process.

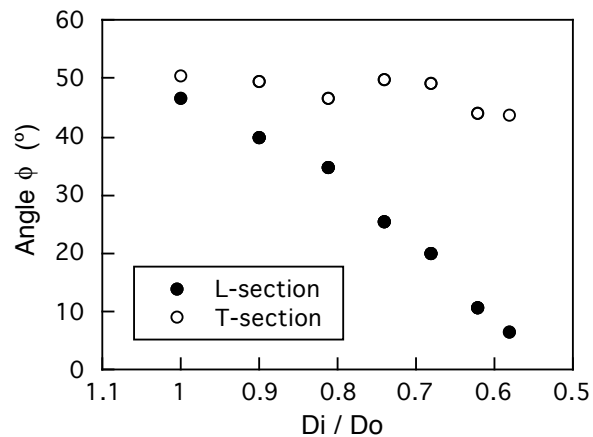


Fig. 17. Orientation angles of the lamellae for different degrees of cold drawing.

Microstructure and macroscopic stress-corrosion behaviour

Hydrogen assisted cracking (HAC).

The HAC tests on pearlitic steel wires with different degrees of cold drawing are described in [27]. After the experiments, a progressive change in the macroscopic topography as the cold drawing increases was observed in all fracture surfaces. Fig. 18 offers a 3D-view of the fracture surfaces and Fig. 19 shows the procedure for measuring the geometric parameters of the crack path in the two obtained cases of mode I crack growth and mixed mode propagation.

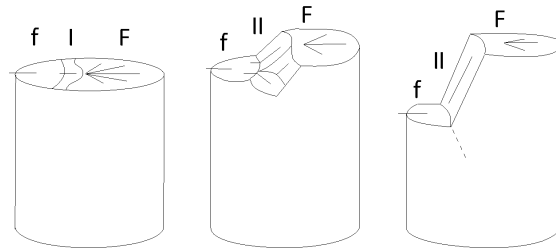


Fig. 18. Evolution with cold drawing of fracture surfaces in HAC, from slightly to heavily drawn steels (left to right). Increasingly anisotropic behaviour with cold drawing (f: fatigue; I: mode I propagation; II: mixed mode propagation; F: final fracture by cleavage).

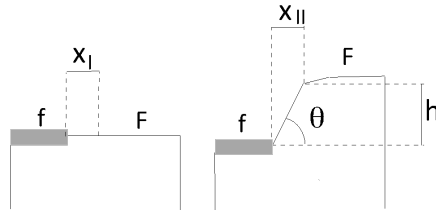


Fig. 19. Geometric parameters describing the fracture path in HAC: slightly drawn steel (left) and heavily drawn steel (right).

It is seen that mixed mode crack growth appears from a certain cold drawing level, and is associated with crack deflection which starts just at the tip of the fatigue precrack, i.e., a deviation in the crack growth path, from its initial fatigue crack growth path, appears at the very beginning of the HAC test. In the first steps of cold drawing the crack growth develops in mode I in both fatigue precracking and hydrogen-assisted cracking. In steels with an intermediate degree of drawing, there is a slight deflection in the hydrogen-assisted crack, and this deflection is not uniform along the crack front but produces a wavy crack at different levels, and finally returns to the direction perpendicular to the wire axis. For the most heavily drawn specimens the crack deflection takes place suddenly after the fatigue precrack and the deviation angle is higher and more or less uniform along the whole crack front. In these last stages of cold drawing, not only crack deflection but also crack branching is observed just after the fatigue precrack tip, i.e., there are two predamage directions (crack embryos), only one of which becomes the final fracture path.

Localized anodic dissolution (LAD).

The LAD tests on pearlitic steel wires with different degrees of cold drawing are described in [28]. After the tests, a progressive change in the macroscopic topography as the cold drawing increases was observed in all fracture surfaces. Fig. 20 offers a 3D-view of the fracture surfaces and Fig. 21 shows the procedure for measuring the geometric parameters of the crack path in the cases of mode I and mixed mode.

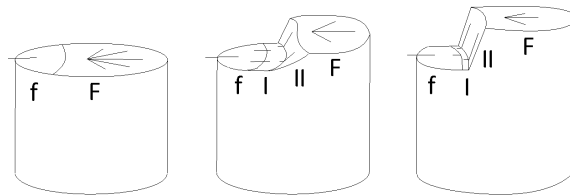


Fig. 20. Evolution with cold drawing of fracture surfaces in LAD, from slightly to heavily drawn steels (left to right). Increasingly anisotropic behaviour with cold drawing (f: fatigue; I: mode I propagation; II: mixed mode propagation; F: final fracture by cleavage).

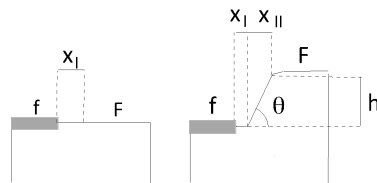


Fig. 21. Geometric parameters describing the fracture path in LAD: slightly drawn steel (left) and heavily drawn steel (right).

In slightly drawn steels, the fracture surfaces were plane and oriented perpendicularly to the loading axis. In the steels with intermediate and high levels of cold drawing, the macroscopic fracture profile presents three characteristic zones, as sketched in Fig. 20. After the fatigue precrack there is a first propagation in its own plane (mode I cracking) over a distance x_I ; after this the crack changes its propagation direction and a mixed mode propagation takes place over a distance x_{II} (measured as the horizontal projection); finally the crack path follows the original direction up to final fracture. For heavily drawn steels the mode I propagation distance decreases as the cold drawing degree increases, the step appears earlier and is associated with increasing values of the angle θ and the step height h , i.e., the crack growth path approaches the drawing direction.

Materials science approach.

The experimental results showed a fundamental fact in both HAC and LAD: the stress-corrosion behaviour becomes more anisotropic as the degree of cold drawing increases, so a transverse crack tends to change its propagation direction to approach that of the wire axis, and thus a mode I growth evolves towards a mixed mode propagation.

It may be assumed that the microstructural orientation in drawn steels influences their macroscopic behaviour, so the resistance to stress corrosion cracking is a directional property depending on the microstructural orientation in relation to the cold drawing direction (strength anisotropy with regard to stress corrosion cracking).

The research in papers [27, 28] establishes a link between the steel microstructure (progressively oriented as a consequence of cold drawing) and its macroscopic stress corrosion behaviour (increasingly anisotropic as the degree of cold drawing increases).

Fig. 22a shows a plot of the evolution of the orientation angles of the pearlitic colonies and lamellae with cold drawing (angle α between the transverse axis of the wire and the major axis of the pearlite colony, modelled as an ellipsoid, angle α' between the transverse axis of the wire and the direction marked by the pearlite lamellae in the longitudinal metallographic section).

In both cases there is an increasing trend with cold drawing, i.e., both the pearlite lamellae and the pearlitic colonies become increasingly aligned in the cold drawing direction. The angles α and α' are measured from the radial direction (the direction of the initial crack in mode I) in the fracture mechanics sense, i.e., they are the complementary angles of those measured in the metallographic L-sections (as indicated in Figs. 15 and 17).

Fig. 22b shows the evolution with cold drawing of macroscopic parameters characteristic of the crack path (fracture profile) in the HAC tests, and Fig. 22c shows the same in the LAD tests. The behaviour is qualitatively similar in both, i.e., isotropic or quasi-isotropic in the slightly drawn steels and increasingly anisotropic with cold drawing.

The important difference is that the material is able to undergo mode I cracking in LAD conditions, even for the heavily drawn steels, although when the crack deflection appears, the mode I propagation distance is a decreasing function of the degree of cold drawing.

As shown in Fig. 22, the progressive microstructural orientation (at the two levels of colonies and lamellae) clearly influences the angle and height of the fracture step (increasing with the degree of cold drawing in both HAC and LAD) and the mode I distance in LAD (decreasing with it in the case of heavily drawn steels).

The change in crack propagation direction can be considered as the proof of the microstructurally-induced strength anisotropy in these materials: from a certain degree of cold drawing the cracks find propagation directions with lower stress corrosion resistance (the same happened in the case of fracture processes in air).

The previous considerations suggest that the macroscopic environmentally assisted fracture behaviour of the different steels (progressively anisotropic with cold drawing) is a direct consequence of the microstructural evolution towards an oriented arrangement.

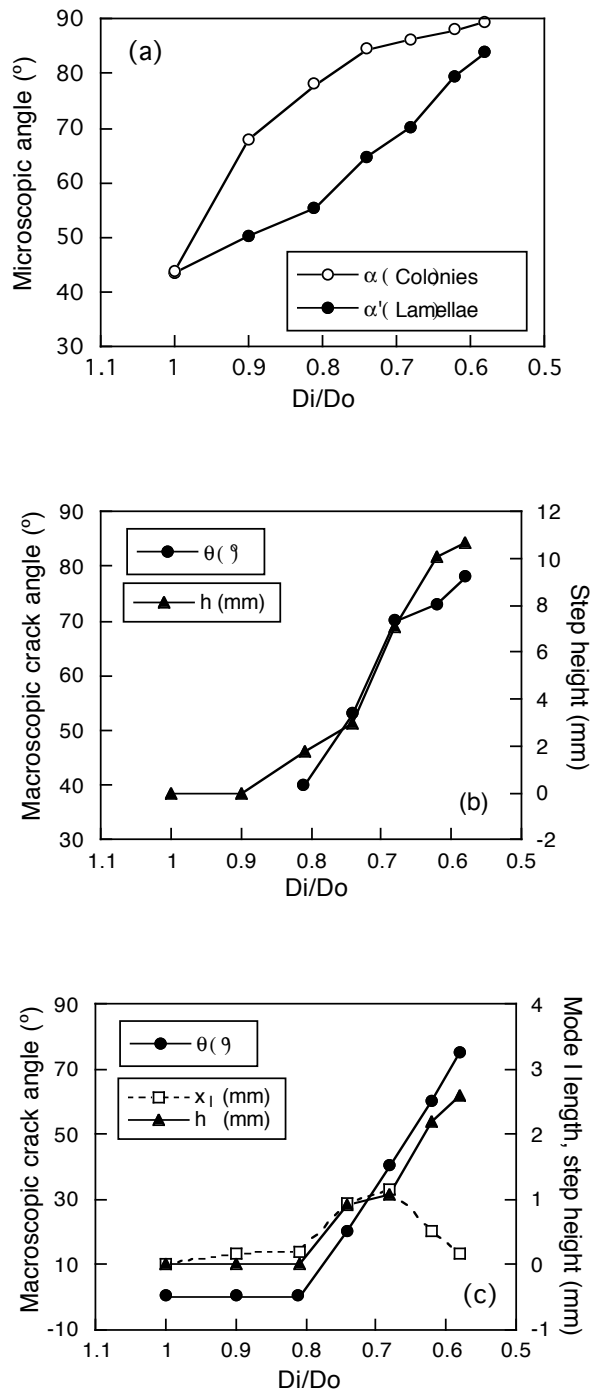


Fig. 22. Relationship between microstructure and macroscopic stress-corrosion behaviour: (a) evolution with cold drawing of the orientation angles of colonies and lamellae in the pearlitic microstructure; (b) evolution with cold drawing of the macroscopic crack angle and step height in HAC conditions; (c) evolution with cold drawing of the macroscopic crack angle, step height and mode I propagation distance in LAD conditions; the angles α , α' and θ are measured from the radial direction (transverse to the wire axis).

Fracture mechanics approach to hydrogen assisted cracking: analysis of the K -dominance condition

This section of the present review paper summarizes the achievements of a basic research line in the field of environmentally assisted cracking in general and of hydrogen degradation in particular. It deals with the meaning and significance of the fracture mechanics approach to hydrogen assisted cracking, analyzing the question of K -dominance not only over the purely mechanical aspects, but *also* over the environmental (physico-chemical) events influencing the whole coupled process of hydrogenation and failure.

Two key factors able to violate the uniqueness of the crack growth kinetics curve $v = v(K)$ are discussed: the role of *far field* (the stress-strain field which is not K -dominated) and the effect of the *history* of hydrogenation and crack growth. Stress-strain assisted diffusion of hydrogen is considered as the rate-controlling factor of hydrogen assisted cracking under sustained or quasi-static loading conditions. The far field is shown to have a minor effect on near-tip hydrogen diffusion. It can only widen the scatter band of crack growth rates in the near-threshold portion of the $v(K)$ -curve.

With regard to the effect of history, the study reveals that hydrogenation and crack growth are coupled processes, one influencing the other, so the crack growth kinetics curve $v = v(K)$ is not unique as an intrinsic material property must be. However, a special regime of steady-state crack growth is seen to exist in which hydrogen assisted cracking turns out to be a K -dominated process, and the corresponding plot of the steady-state v against K acquires the uniqueness of a material's characteristic curve which may be used in engineering to provide more conservative evaluation of material resistance and structural integrity.

Introduction.

Engineering design frequently involves problems of environmentally assisted cracking (EAC) in materials and structures, a phenomenon which appears in diverse forms such as stress corrosion cracking, hydrogen assisted cracking (HAC), etc. In this framework, the fracture mechanics approach is effective for material evaluation and structural integrity assessment.

In the domain of linear elastic fracture mechanics under small scale yielding, the stress intensity factor K is the only parameter governing the stress-strain state in the vicinity of the crack tip. The key of the fracture mechanics approach to EAC is the *crack growth kinetics curve* (Fig. 23): a plot of crack growth rate v vs. stress intensity factor K , defined between the threshold K_{th} (below which the crack growth rate v is zero) and the fracture toughness K_c .

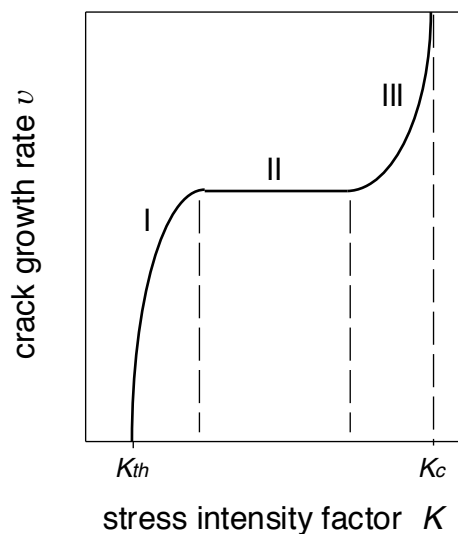


Fig. 23. Scheme of a typical crack growth kinetics curve with three stages: near-threshold (I), plateau (II) and mechanical final fracture (III).

The idea of *uniqueness* of $v(K)$ -curves and thresholds K_{th} as intrinsic characteristics of {material-environment} systems forms the backbone of the approach and ensures the soundness of applications in engineering design. This uniqueness ensures the *similitude* of crack behaviour in test specimens and in structural components in service, thereby providing *transferability* of laboratory testing data to real engineering structures.

If the $v(K)$ -curve including K_{th} is indeed unique for a given {material-environment} couple, any discrepancy between predicted and real behaviour should be attributed to roughness in the analysis or experimental scatter but not to the concept. Otherwise, conceptual weakness makes the predictions less reliable and calls for more constraints on testing and evaluation to obtain data of the crack growth resistance parameters in an aggressive environment.

The reliability of the fracture mechanics approach to EAC in engineering design was reviewed in [29], where an ample range of experimental evidence of uncertainty in the $v(K)$ -curve and the threshold K_{th} is presented. Although these items are supposed to depend solely on the material and the environment, they are notably sensitive to the influence of a wide family of test/service variables, namely the following (cf. [29]):

- (i) *pre-loading*: fatigue pre-cracking regime and overloads;
- (ii) *geometry*: crack length, crack bluntness and stress intensity gradient;
- (iii) *kinematics*: initial load, test interruption, rate of loading/straining.

The results quoted show that the same stress intensity factor does not always yield equal crack velocities in otherwise identical couples {material-environment}. The observed deviations cannot be related to imperfect testing and are systematic as distinct from obvious statistical scatter of test data. This uncertainty of the basic fracture mechanics characteristics of EAC produces loss of confidence in materials evaluation and structural integrity assessment.

In paper [30], a deal of uncertainty of EAC characterisation is eliminated in a strictly *local* fracture mechanics approach where both the mechanical and the environmental factors are treated in terms of local variables related to the crack tip. However, this local interpretation of the crack growth kinetics curve still remains incomplete and does not meet the essential requirements of an intrinsic material curve.

To solve the problem, a procedure is proposed in [30] for engineering safe design against EAC. For a given {material-environment} system, the aim is to find the *worst* crack tip situation producing the fastest crack growth rate v_m attainable at each K . The corresponding master curve $v_m(K)$ is the envelope of all possible $v(K)$ -curves for a {material-environment} couple and represents an intrinsic characteristic of the system: the weakest resistance to EAC.

However, the extent to which the $v(K)$ -curve and the threshold K_{th} are the properties of only the material and the environment becomes an open issue. This kind of uncertainty means that the process in general is not exclusively K -dominated, although no attempt has been made in the past to elucidate the matter of K -dominance over the whole family of contributing events as the check-point for the soundness of the fracture mechanics approach to EAC.

The present paper reviews some recent research work by the authors on the meaning and significance of the fracture mechanics approach to the particular phenomenon of HAC (very important in engineering). The final aim is to elucidate the question of K -dominance not only over the mechanical aspects of the phenomenon but *also* over the environmental (physico-chemical) events affecting the coupled process of hydrogenation and failure.

Meaning and significance of the fracture mechanics approach to HAC

Key events of HAC

The main events associated with HAC are [31]:

- (i) hydrogen supply to the prospective fracture places, involving hydrogen transport to metal, entry into it and transport within it;
- (ii) stress-strain state as mechanical impetus for hydrogen assisted damage;
- (iii) damage enhancement by hydrogen.

Crack tip hydrogen activity may be presented in terms of its partial pressure P^{CT} in gaseous environments or the electrode potential E_v^{CT} and the hydrogen ion exponent pH^{CT} in corrosive conditions (all referred to the crack tip zone). They can significantly differ from P or E_v and pH (characteristics of the bulk environment). Relations of bulk and local environment parameters are governed by in-crack environmental currents and kinetic processes of mass-charge exchange and chemical reactions (Fig. 24). Thus, local environmental variables depend on the geometry of the crack and on time t :

$$P^{CT} = P^{CT}(P, a, \delta, t) \quad (1)$$

in gaseous environments, or

$$pH^{CT} = pH^{CT}(pH, E_v, a, \delta, t) \quad (2)$$

$$E_v^{CT} = E_v^{CT}(pH, E_v, a, \delta, t) \quad (3)$$

in corrosive ones, where the geometry parameters a (crack depth) and δ (the height of an opened crack) represent the characteristic transportation distance from bulk environment to the crack tip (here only the crack depth is taken for the sake of simplicity) and crack opening displacement under load which gives the canal width (variable along crack faces). The right hand parts of relations (1) and (2)-(3) in general are not plain functions of instantaneous values of displayed variables but functionals over their time histories depending, in particular, on the shapes of entire trajectories $a(\tau)$ and $\delta(\tau)$ in the time interval $0 \leq \tau \leq t$. This implies the influence of both loading/cracking history and crack geometry outside the K -controlled crack tip zone on the near tip environment, and therefore, on the value of v at given K under fixed bulk environment.

The phase of hydrogen entry into metal includes physical adsorption of hydrogen-containing species on metal surface; dissociative chemisorption of atomic hydrogen and its dissolution in the surface layer. The surface phase of sorption may be the rate determining step for HAC under relatively weak hydrogenation conditions at the crack tip, but this is unusual for most practical cases of gaseous or electrochemical (corrosive) hydrogenation when at entry sites elevated hydrogen activity is achieved (cf. [31]).

With regard to the phase of hydrogen transport towards the prospective fracture nuclei, two transport modes must be distinguished, as explained above (cf. first main section): *diffusion* and *transport by moving dislocations*. Under sustained or quasi-static loading, local over-saturations due to hydrogen supply by dislocations have time to be reduced by short-range diffusion, and thus the significance of dislocational transport seems to be negligible in this case. Then the long-range (in relative scale) diffusion driven by macroscopic stress-strain field is the main operative mode of hydrogen transport to fracture nuclei in metals. This transport step is frequently the slowest one among all the phases of hydrogen transportation, and thus the kinetics of hydrogen assisted fracture is often diffusion controlled.

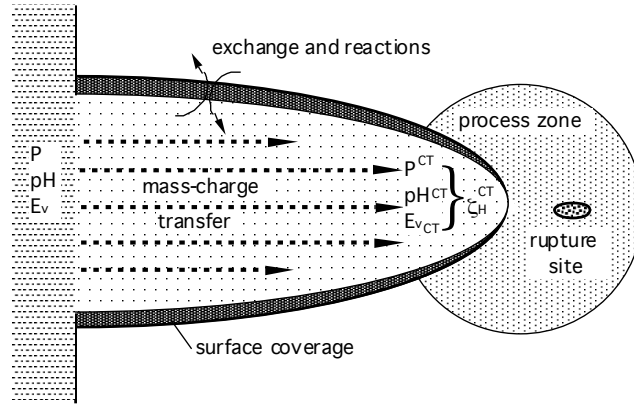


Fig. 24. In-crack environmental currents and kinetic processes of mass-charge exchange and chemical reactions.

Modelling of the HAC process

Hydrogen promotes failure by different physical mechanisms (cf. [31]) so that elementary fracture events are associated with a critical combination of hydrogen concentration C and mechanical variables representing the stress-strain state. The latter determines the critical value of hydrogen concentration C_{cr} to complete local fracture. Thus, the critical situation occurs when hydrogen concentration in prospective rupture sites reaches a critical value dependent on the mechanical action in the fracture process zone:

$$C = C_{cr} \quad (4)$$

The *critical* concentration of hydrogen is a function of the mechanical situation (stress-strain state) at a material point, i.e.:

$$C_{cr} = C_{cr}(\sigma, \varepsilon_p) \quad (5)$$

where $\sigma = \sigma(r, t)$ and $\varepsilon_p = \varepsilon_p(r, t)$ are respectively the tensors of stress and plastic strain, r being the spatial coordinate vector and t the time. Throughout this section of the paper, a solid subjected to *sustained loading conditions* will be analyzed and in this case the tensors of stress and strain depend only on the spatial coordinate: $\sigma = \sigma(r)$ and $\varepsilon_p = \varepsilon_p(r)$.

The *actual* concentration, depending on the specific location of the material point and on time, is itself a function of the stress-strain state:

$$C = C(r, t; \sigma, \varepsilon_p) \quad (6)$$

Hydrogen entry can be characterised by the equilibrium value C_Γ of hydrogen concentration in stressed-strained metal at the entry surface Γ (boundary between the metal and the environment):

$$C(\Gamma, t) = C_\Gamma \quad (7)$$

The driving force for diffusion X_D is determined by the gradient ∇ of its chemical potential μ_H :

$$X_D = -\nabla\mu_H \quad (8)$$

which is related to the solubility coefficient K_S (density of available sites) for hydrogen in metal:

$$\mu_H = RT \ln \frac{C}{K_S} \quad (9)$$

where R is the ideal gas constant and T the absolute temperature. The solubility K_S depends on temperature, *hydrostatic stress* σ , alloy microstructure, chemical and phase composition of the alloy and hydrogen traps density (traps for hydrogen in metals are formed by lattice imperfections; dislocations are nearly the strongest kind of traps but not the only ones). The overall density of traps depends on the plastic strain level which may be represented by the second invariant of the plastic strain tensor: the *effective or equivalent plastic strain* ε_p . In addition, plastic strain may affect the phase composition of an alloy, thereby causing variations of hydrogen solubility, as in austenitic steels through strain-induced $\gamma \rightarrow \alpha$ transformation. Thus, plastic strain is another variable affecting hydrogen solubility in metal, in addition to hydrostatic stress and temperature:

$$K_S = K_S(\sigma, \varepsilon_p, T) \quad (10)$$

The latter may be decomposed into its plastic strain dependent part $K_{S\varepsilon}$ and the hydrostatic stress related one (cf. [31]):

$$K_S(\sigma, \varepsilon_p, T) = K_{S\varepsilon}(\varepsilon_p, T) \exp(\Omega\sigma) \text{ with } \Omega = \frac{V_H}{RT} \quad (11)$$

where V_H is the partial molar volume of hydrogen in metal.

The gradient (inhomogeneity) of any of the solubility-affecting factors can induce diffusion flux. On assuming *uniform temperature distribution* in the solid (a hypothesis maintained throughout this paper) the diffusion flux J may be expressed as follows:

$$J = \frac{D}{RT} C X_D = -DC \nabla \ln \frac{C}{K_S} \quad (12)$$

where D is the diffusion coefficient of hydrogen in metal which characterises the specie mobility; the diffusivity should not be treated as a constant but considered to be dependent on plastic strain: $D = D(\varepsilon_p) \neq \text{const}$, to reflect the influence of the altered phase composition or trap density on the averaged (macroscopic) mobility of diffusable species (cold work effect), apart from their effect on solubility reflected in equations (10) and (11). Substitution of (11) into (12) yields:

$$\mathbf{J} = -D(\varepsilon_p) \left\{ \nabla C - C \left[\nabla(\Omega\sigma) + \frac{\nabla K_{S\varepsilon}(\varepsilon_p)}{K_{S\varepsilon}(\varepsilon_p)} \right] \right\} \quad (13)$$

The condition of mass balance gives the diffusion equation in terms of concentration as:

$$\frac{\partial C}{\partial t} = -\text{div } J \quad (14)$$

which allows an evaluation of concentration evolution with time t . According to (13) and (14), the equation of stress-*and*-strain assisted diffusion in terms of concentration takes the form:

$$\frac{\partial C}{\partial t} = D [\nabla^2 C - M \cdot \nabla C - NC] + \nabla D \cdot [\nabla C - MC] \quad (15)$$

where the dot \cdot denotes scalar product and the coefficients M and N are:

$$M = \nabla \ln K_S(\sigma, \varepsilon_p); N = \nabla^2 \ln K_S(\sigma, \varepsilon_p) \quad (16)$$

The hydrogen entry into metal is characterised by the *boundary condition* for diffusion (7) with $C_r = C_0 K_S(\Gamma)$, where C_0 is the equilibrium hydrogen concentration provided by the environment in the bare metal (free of stress and plastic strain). Accounting for (11), it yields the following:

$$C_r = C_0 K_S(\Gamma) = C_0 K_{S\sigma}(\varepsilon_p(\Gamma)) \exp(\Omega\sigma(\Gamma)) \quad (17)$$

For solids under conditions of uniform environmental hydrogen activity characterised by an equilibrium concentration value $C_0 = \text{const}$, it is easy to get the exact *steady-state solution* of equation (15) of stress-strain assisted diffusion which is asymptotically attained at $t \rightarrow \infty$. This corresponds to the equilibrium state when the diffusion flux (12) is zero or, equivalently, when the diffusion driving force (8) is null. According to expression (12), this is provided when $C/K_S = \text{const}$. Then, taking into account relation (11), the steady-state solution is the following:

$$C_{\infty}(r) = C_0 K_S(r) = C_0 K_{S\varepsilon}(\varepsilon_p(r)) \exp(\Omega\sigma(r)) \quad (18)$$

With $\varepsilon_p = 0$, $K_{S\varepsilon} = 1$ and the last expression coincides with the well known one for stress-only driven concentration.

Fracture mechanics approach to HAC

The basic concept of mechanical autonomy of the crack tip region (K -dominance) is the keystone of the linear elastic fracture mechanics approach [31]. It may be interpreted as follows: there is a region of characteristic size R_{SIF} (Fig. 25) around the crack tip where the elastic stress-strain state is K -dominated, i.e., adequately represented *solely* by the universal $r^{-1/2}$ singular term of the complete series solution. This is the asymptotic term σ_a of hydrostatic stress if one focuses on this component (the relevant one in hydrogen diffusion).

In addition, a nonlinear region (the fracture process zone of size R_{FPZ}) does exist in the vicinity of the crack tip where microscopic damage proceeds, and it is usually surrounded by the plastic region of size R_Y . The whole inelastic zone (fracture process zone plus plastic region) may be so small that it does not sensibly disturb the linear elastic solution (*small scale yielding* condition). If this happens, the K -dominated annular elastic region still exists at distances from crack tip $R_Y < r \leq R_{\text{SIF}}$. Outside this annular domain (at $r > R_{\text{SIF}}$) the remote stress-strain field (*far field*) is not governed by K , nor is its hydrostatic component σ_f in particular.

As far as this K -dominated ring shields completely the inelastic zone from any other external influence, except that provided by K , it means that the state of the whole inelastic near-tip region including the fracture process zone depends solely on K and material, i.e., it is also autonomous and thus the stress intensity factor K is the parameter governing the crack tip mechanical pre-damaged state, despite the lack of explicit treatment of nonlinear behaviour and microfracture events in the fracture process zone.

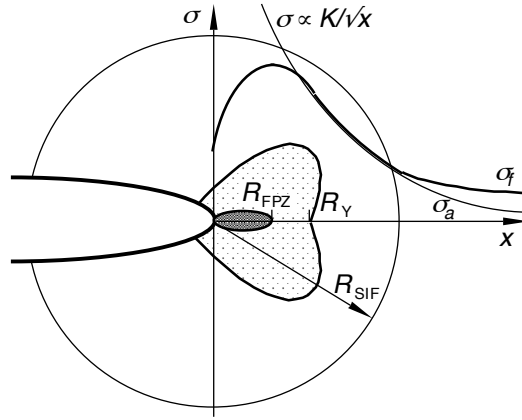


Fig. 25. Specific zones and stress state in the vicinity of the crack tip.

In the matter of HAC, when a crack of depth a is present in the material, the hydrogen assisted fracture criterion (4) remains valid. Considering the K -dominance over the stress-strain state in the vicinity of the crack tip, the *critical* concentration (5) is a function of the stress intensity factor K in this case:

$$C_{cr} = C_{cr}(\sigma(K, r), \varepsilon_p(K, r)) \quad (19)$$

and the *actual* concentration (6) yields:

$$C = C(r, t; \sigma(K, r), \varepsilon_p(K, r)) \quad (20)$$

In terms of independent variables only and using the local coordinate x with origin at the crack tip (Fig. 25):

$$C_{cr} = C_{cr}(K, x) \quad (21)$$

$$C = C(x, t; K) \quad (22)$$

Thus, to have K -dominance over the whole HAC process, and thus uniqueness of the $v(K)$ curve as an attribute of a given {material-hydrogen} system, two preconditions must be fulfilled:

/1/ K -controlled uniqueness of critical hydrogen concentration C_{cr} which must be reached at some point of the fracture process zone to cause local fracture and crack advance;

/2/ K -dominance over the process of hydrogenation in the fracture process zone ahead of the crack tip, i.e., uniqueness of the evolution of the distribution of hydrogen concentration $C(x, t)$.

According to criterion (4) the curves given by the right-hand parts of equations (21) and (22) should meet at some point to cause crack extension. Achievement of exclusive K -dominance over the solution of this problem of contact between two curves (of *critical* and *actual* hydrogen concentrations) requires K -control over the curves themselves in the close vicinity of the instantaneous crack tip.

Since the critical concentration C_{cr} in the vicinity of the crack tip inherits the property of K -dominance from the stress-strain fields, the two preconditions /1/ and /2/ formulated above are equivalent to the following ones:

/1*/ K is the only variable which controls the near-tip stress-strain fields (i.e., $\sigma = \sigma(K, r)$ and $\varepsilon_p = \varepsilon_p(K, r)$) in a domain embracing the physical process zone, thus dominating the mechanical aspects of both pre-damage and stress-strain affected hydrogenation;

/2*/ in addition, K also governs the environment parameters which control hydrogenation in the very close vicinity of the crack tip (*local* environment parameters) which determine the hydrogen concentration evolutions $C(x,t)$ in the fracture process zone.

Finally, the two preconditions may be formulated in terms of fracture mechanics concepts as follows:

/1**/ K -controlled *mechanical autonomy* of the crack tip region, i.e., K -dominance over the stress-strain field, which is the keystone of linear elastic fracture mechanics under small scale yielding;

/2**/ K -controlled *environmental autonomy* of the crack tip region, i.e., K -dominance over the physico-chemical events, namely the boundary conditions and the hydrogen diffusion in the vicinity of the crack tip.

While the first precondition is always fulfilled in the framework of linear elastic fracture mechanic analyses under small scale yielding, the achievement of the second one is not guaranteed in all cases, because many causes may destroy the K -dominance in HAC (cf. [31]) and thus the uniqueness of the crack growth kinetics curve $v=v(K)$. In further sections of this paper, the effects of far field and history are discussed in depth.

However, in spite of the fact that the $v(K)$ -curve is not always K -dominated (the second precondition could fail), on assuming sustained loading conditions (as in the approach presented in this paper) the threshold K_{th} always meets the two preconditions of K -dominance, because the limit of crack non-propagation is associated with the unique steady-state distribution of concentration $C_{\infty}(r)$ near a tip of a stationary crack reached at $t \rightarrow \infty$. This stationary solution of the equation of stress-strain assisted diffusion was given in (18) and it has the same self-similitude properties as the stress-strain field. Therefore, only the first precondition (mechanical autonomy) is necessary to guarantee the uniqueness of the threshold state which is always K -dominated when linear elastic fracture mechanics, small scale yielding and sustained loading are considered.

The effect of far field on K -dominance in hydrogen assisted cracking

The effect of far field on stress-strain assisted diffusion

The matter of K -dominance with regard to hydrogen diffusion in the near-tip region is addressed in paper [32]. It is the question of the accuracy of the approximate hydrogen concentration distribution C_a governed by the K -dominated component of the near-tip stress-strain field (i.e., by the *asymptotic* term σ_a) to represent the actual concentration C_f being driven by the complete mechanical field containing the whole series expansion (i.e., influenced by the non-autonomous *far field* σ_f). To this end, the discrepancy $\mathcal{E} = C_a - C_f$ between the two concentration distributions is the subject of interest to estimate the effect of the far field (the remote stress-strain field which is not K -controlled) on hydrogenation of the fracture process zone.

In accordance with the general form of the equation of stress-strain assisted diffusion (15), the equations to obtain the far-field affected concentration C_f (exact) and the near-tip asymptotically driven one C_a (approximate) are the following:

$$\frac{\partial C_f}{\partial t} = D [\nabla^2 C_f - M_f \cdot \nabla C_f - N_f C_f] + \nabla D \cdot [\nabla C_f - M_f C_f] \quad (23)$$

$$\frac{\partial C_a}{\partial t} = D [\nabla^2 C_a - M_a \cdot \nabla C_a - N_a C_a] + \nabla D \cdot [\nabla C_a - M_a C_a] \quad (24)$$

where the coefficients M and N with subindices f and a are determined according to formulae (16) by their corresponding mechanical fields (the complete and the asymptotic ones).

Accounting for the small scale yielding condition, near the crack tip there is a K -dominated region ($r < R_{\text{SIF}}$) where the two elastoplastic stress-strain fields coincide. In addition, plasticity is assumed to be associated solely with the crack tip region and no other plastic zones exist. Correspondingly, inelastic behaviour is always K -governed and plastic strain ε_p does not participate in equations (23)-(24) as a matter of distinction. Thus, the difference is related to the discrepancy between the two hydrostatic stress fields: the far field σ_f and the asymptotic one σ_a at $r > R_{\text{SIF}}$.

Subtracting one of the above equations from another the following equation can be derived with regard to discrepancy:

$$\frac{\partial \mathcal{E}}{\partial t} = D [\nabla^2 \mathcal{E} - M_f \cdot \nabla \mathcal{E} - N_f \mathcal{E}] + \nabla D \cdot [\nabla \mathcal{E} - M_f \mathcal{E}] + Q \quad (25)$$

where an additional source-type term arises (cf. [32]):

$$Q = \begin{cases} D \Omega \nabla (\sigma_f - \sigma_a) \cdot \nabla C_a \neq 0 & \text{at } r > R_{\text{SIF}} \\ 0 & \text{at } r \leq R_{\text{SIF}} \end{cases} \quad (26)$$

This expression represents the source term for diffusion of discrepancy \mathcal{E} which is the difference between the approximate K -driven concentration distribution and the exact far-field affected one. With nil initial and boundary conditions for \mathcal{E} , its absolute value increases from zero with time since the source Q produces this imaginable "diffusible substance" in the solid. This "error" is generated by the source Q operative at $r > R_{\text{SIF}}$, and it diffuses from there towards the fracture process zone. The effect of the far field on K -dominance over hydrogen accumulation in the fracture process zone becomes more severe when a greater amount of "error" \mathcal{E} can reach the region $r < R_{\text{FPZ}}$ by "virtual" diffusion from the distant source (26) situated at $r > R_{\text{SIF}}$.

Assessment of K -dominance conditions

After estimation of the sizes of the crack tip zones represented in Fig. 25, and theoretical analysis of the near-tip hydrogen diffusion (for details see [32]), it was possible to obtain the time evolution of the asymptotic (K -driven) concentration C_a at the outer border of the fracture process zone where the effect from the source Q appears first, i.e., at $x = R_{\text{FPZ}}$ as:

$$C_a(x=R_{\text{FPZ}}, t) = C_a(\tau) = C_{\infty}(R_{\text{FPZ}}) \operatorname{erfc} \left(\frac{1}{2\sqrt{\tau}} \right) \quad (27)$$

where $\operatorname{erfc}(\bullet)$ is the complementary error function and τ the dimensionless time defined as $\tau = Dt/R_{\text{FPZ}}^2$.

Fig. 26 shows a plot of this function $C_a(\tau)$ (solid line). Approximately for $\tau \geq 130$, the concentration C_a in the fracture process zone (i.e., for $x \leq R_{\text{FPZ}}$) exceeds 95% of the steady-state level C_{∞} . From then on, its further variation lies within a 5%-scatter band near this hydrogenation limit, i.e., the increase of K -driven concentration in the fracture process zone falls into this 5% strip from the time moment t_{SS} (where the subindex *ss* indicates steady-state) given by:

$$t_{\text{SS}} = 130 \frac{R_{\text{FPZ}}^2}{D} \quad (28)$$

On the other hand, the time t_Q^* at which the source Q becomes noticeable is [32]:

$$t_Q^* \geq t_{SS} \left(\frac{1}{16.1} \frac{R_{SIF}}{R_{FPZ}} \right)^2 \quad (29)$$

Estimating the ratio R_{SIF}/R_{FPZ} from fracture mechanics assumptions, it yields:

$$t_Q^* > t_{SS} \quad \text{if} \quad E/\sigma_Y > 161 \quad (30)$$

where E is the Young modulus and σ_Y the yield stress of the material.

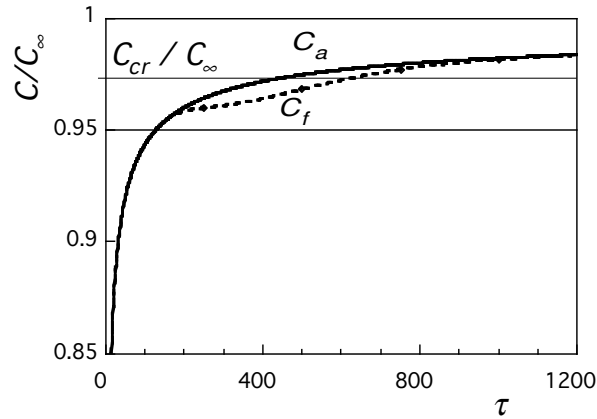


Fig. 26. Plot of hydrogen concentration evolutions with time: asymptotically-driven (K -controlled) concentration C_a (solid line) and a representative of the family of far-field affected concentration C_f (dashed line). An example of near-threshold critical concentration level C_{cr} below the steady-state one C_∞ at K_{th} is also shown.

Thus the far field can affect the K -driven hydrogenation of the fracture process zone well after the transient concentration falls within a 5% scatter band near the steady-state hydrogen distribution in that area. Within the narrow 5%-width strip in the vicinity of the steady-state limit C_∞ which defines K_{th} by criterion (4) the supposition about K -control over hydrogen diffusion may be erroneous, as shown in Fig. 26 where the dashed line represents schematically one of the possible C_f -curves. This fact can affect the $\nu(K)$ -curve only in its near-threshold part, but without affecting the threshold itself which remains K -controlled (cf. [32]).

The effect of history on K -dominance in hydrogen assisted cracking

Neither of the two processes of crack propagation and hydrogen diffusion should be considered separated from the other, since the movement of a crack tip is relevant to hydrogen accumulation in the fracture process zone. In terms of the theory of boundary value problems this situation is qualified as diffusion with moving boundary. Thus the crack growth history appears as a factor capable of affecting near tip diffusion and consequently the kinetics of HAC, apart from the stress-strain field represented by K . This again questions the idea of exclusive K -dominance over HAC.

The effect of history of the coupled hydrogenation-cracking process on K -dominance during HAC is addressed in previous research work [33, 34]. Paper [33] develops theoretical bases and a qualitative analysis demonstrating the coupling between hydrogenation and crack growth, so that the crack growth rate in HAC generally is not governed solely by K . The quantitative consideration is given in [34] where the K -dominance condition is analyzed, showing the significance of the history effect

which destroys K -control over crack growth rate, although a special regime of steady-state crack growth is seen to exist for which hydrogen assisted cracking becomes a K -dominated process.

Coupling of hydrogenation and crack growth

In this section, the HAC process is analyzed in a *moving crack*. As in the rest of this paper, the analysis is focussed on sustained or quasi-static loading. The small scale yielding condition near the crack tip is assumed to be valid for the whole cracking process, so that the K -controlled mechanical autonomy of the near-tip region is supposed to be constantly preserved during crack growth. Adopting the framework of the diffusional theory of HAC outlined in previous sections, the analysis is confined to the *stress-strain* assisted diffusion as the responsible factor of HAC.

With regard to cracking, two approaches can be considered. According to one of them, crack growth proceeds discontinuously by a series of jump-like steps. The time intervals Δt between discrete crack increments Δa are just the periods of accumulation in the fracture process zone of the amount of hydrogen necessary to satisfy criterion (4). The crack growth rate is defined as:

$$v = \Delta a / \Delta t \quad (31)$$

Following the other approach, crack growth is assumed to go on continuously provided that criterion (4) is constantly fulfilled at a distance x_c . The instantaneous crack growth rate is defined here as:

$$v = da / dt \quad (32)$$

These approaches (jump-like and continuous) are usually considered to be essentially different with respect to background physics. Despite numerous speculations trying to support one or other on the basis of physical reasoning, none is generally accepted as adequate to represent the crack growth process.

Jump-like (discontinuous) modelling of crack growth is employed in Fig. 27 which shows schematically the hydrogen concentration curves near the crack tip after successive crack increments. The critical point x_c is supposed for definiteness to coincide with the location at which hydrogen concentration and stress are maxima. Critical concentration must be attained at this point to produce a local rupture event causing jump-like crack increment. All the variables are supposed to be determined *solely* by material properties and K , i.e., they remain constant if $K = const$. Crack propagation consists of a series of loops (cycles) "hydrogen accumulation–local rupture–crack advance".

During each hydrogenation-fracturing cycle some amounts of hydrogen reach sites of possible subsequent fracture process zones. Thus, initial conditions for hydrogen diffusion within each particular loop are, in general, different from the preceding and subsequent cycles (see Fig. 27). This shows the coupling of hydrogen diffusion and crack growth processes which mutually influence on each other. Near tip hydrogen diffusion depends on the whole HAC history, and in particular on increase of crack size $a = a(t)$ and alterations of stress intensity factor $K = K(t)$. Thus, K -dominance in HAC fails because near-tip diffusion at every instantaneous K proceeds along its specific way which starts at the beginning of a particular HAC run.

Smooth (continuous) modelling of crack growth is useful for analytical consideration of the role of history of the coupled hydrogenation-cracking process in maintaining K -control over all crack tip events. Crack size is assumed to be a smooth function $a = a(t)$, the crack growth rate being its ordinary derivative (32).

By analogy with the actual thermodynamic one, the *fictitious driving force* for diffusion may be formally introduced into equation (36):

$$X_D^* = X_D - \frac{RT}{D} v \quad (37)$$

With the use of expression (34) it yields:

$$X_D^* = -RT \nabla \left[\ln \frac{C}{K_S} + \frac{v}{D} x \right] = -RT \nabla \ln \frac{C}{K_S^*} \quad (38)$$

where the formal solubility-like term is

$$K_S^* = K_S^*(\sigma, \varepsilon_p, v) = K_S(\sigma, \varepsilon_p) \exp\left(-\frac{v}{D} x\right) \quad (39)$$

To obtain some closed-form solutions useful to analyze the effect of history, the matter is simplified here by *neglecting the spatial variability of the hydrogen diffusion coefficient* $D = D(\varepsilon_p)$, i.e., taking D as a constant averaged value of $D(\varepsilon_p)$ over the zone of interest. Following this way, the terms with ∇D do not appear in the diffusion equation:

$$\frac{\partial C}{\partial t} = D \left[\nabla^2 C - M^* \cdot \nabla C - N^* C \right] \quad (40)$$

where vector and scalar coefficients, correspondingly, are the following:

$$M^* = \nabla \ln K_S^*(\sigma, \varepsilon_p, v) \quad (41a)$$

$$N^* = \nabla^2 \ln K_S^*(\sigma, \varepsilon_p, v) \quad (41b)$$

Since near-tip stress-strain field components are controlled by K , these equation coefficients, apart from spatial coordinates, depend parametrically on K and crack growth rate v :

$$M^* = M^*(K, v); N^* = N^*(K, v) \quad (42)$$

Therefore, the solution of this problem depends not only on K , but also on crack growth rate v : $C = C(x, t; K, v)$. Hydrogen concentration in the vicinity of the crack tip is determined by stress-strain assisted diffusion equation (40) with the following *boundary condition*:

$$C(x, t)|_{x=0} = C_\Gamma \quad (43)$$

where surface concentration $C_\Gamma = C_0 K_s|_{x=0} = \text{const}$. In addition, the *initial condition* is:

$$C(x, t)|_{t=0} = C_{t0}(x) \quad (44)$$

Crack growth rate v becomes one more unknown variable which must be found from the solution of the *coupled* problem of hydrogen diffusion and crack growth. To close the system of equations for

this coupled diffusion-cracking process, the criterion of crack growth (4) is employed. Using the distance x_c , the *critical* and *actual* concentrations (21) and (22) become:

$$C_{cr} = C_{cr}(K, x_c) \quad (45)$$

$$C = C(x_c, t; K, v) \quad (46)$$

and the crack growth criterion:

$$C(x_c, t; K, v) = C_{cr}(K, x_c) \quad (47)$$

This formulation of the diffusion-cracking problem is completely closed provided the stress intensity factor K is somehow known. For such a case, if C is a solution of the diffusion equation (40) parametrically dependent on crack growth rate v , the latter can be found from equation (47) as:

$$v = v(K, t) \quad (48)$$

Therefore, the crack growth rate must not be the same at equal values of K , but varies with the total HAC process time t .

However, in most practical situations, K depends on both applied load and crack length, $K = K(a)$, and consequently, the coefficients (42) of the equation (40) do too. Hence, crack length a turns out to be the additional unknown variable to be determined from the solution of the coupled problem. Differential equation (32) concerning crack size has the obvious solution:

$$a(t) = a_0 + \int_0^t v dt \quad (49)$$

The problem is reduced to the same as for $K = const$, but now the equation (47) to determine the crack growth rate with $K = K(a)$ becomes not a function parametrically dependent on v , but a functional over the whole *history* of the process. Correspondingly, crack growth rate as a solution of this coupled diffusion-cracking problem also becomes a functional dependent on a certain process history with its individual $K(a)$ -variation. The variability of crack growth rate at the same K is thus inevitable.

A revision of K-dominance

Using the same formalism as for a stationary crack under sustained load and taking the form of this solution in terms of the solubility coefficient K_s , substituting this by its analogue $K_s^*[\sigma(x; K), \varepsilon_p(x; K), v] = K_s^*(x; K, v)$, an approximate solution for diffusion near a moving crack tip may be built as:

$$C(x, t; K, v) = C_0 K_s^*(x; K, v) \operatorname{erfc}\left(\frac{x}{2\sqrt{Dt}}\right) \quad (50)$$

Taking into account the expression (39) this renders:

$$C(x, t; K, v) = C_0 K_s(x; K) \exp\left(-\frac{v}{D} x\right) \operatorname{erfc}\left(\frac{x}{2\sqrt{Dt}}\right) \quad (51)$$

Using the crack growth criterion (47), it yields an equation which can be solved to obtain the crack growth rate v for a given K :

$$v(K, t) = -\frac{D}{x_c} \ln \left[\frac{C_{cr}(K, x_c)}{C_0 K_S(x_c, K) \operatorname{erfc} \left(\frac{x_c}{2\sqrt{Dt}} \right)} \right] \quad (52)$$

which has physical sense only after some incubation period t_{in} has elapsed, i.e., at $t \geq t_{in}$. For earlier times $t < t_{in}$ it gives negative values of the crack growth rate when the expression in square brackets in formula (52) exceeds unity. This happens for:

$$t_{in} = \frac{1}{4D} \left[\frac{x_c}{\operatorname{erfc}^{-1}(C_{cr}/C_{\infty})} \right]^2 \quad (53)$$

where the function $\operatorname{erfc}^{-1}(\bullet)$ is the one inverse to $\operatorname{erfc}(\bullet)$ and $C_{\infty} = C_0 K_S(x_c, K)$ is the exact steady-state solution for hydrogen diffusion near a stationary crack attained at long time $t \rightarrow \infty$.

For the range $K_{th} \leq K < K_c$ in the $v(K)$ -curve (cf. Fig. 23), the inequality $C_{cr}(K) \leq C_{\infty}(K)$ is valid, i.e., the argument of the function $\operatorname{erfc}^{-1}(\bullet)$ in (53) always lies between 0 and 1 where the function is defined. This is because for HAC to occur, the critical hydrogen concentration C_{cr} must be achieved sooner or later, and the steady-state one C_{∞} is just the maximum concentration which can ever be asymptotically reached at fixed K near a stationary crack.

Fig. 28 gives the time evolution of hydrogen concentration (51) for an initially stationary crack ($v = 0$). After applying the criterion (4), or (47) with $v = 0$, to obtain the instant at which it must start to grow, one obtains exactly the same result as given above in (53) for t_{in} . Thus the meaning of the time limit at which a solution exists for the crack growth rate in the coupled diffusion-cracking problem is just the incubation period before HAC starts to proceed.

From relation (52) it follows that the crack growth rate at fixed K is a rising function of time which starts to increase from $v=0$ at $t=t_{in}$ and asymptotically approaches a *steady-state* value v_{SS} as $t \rightarrow \infty$:

$$v_{SS} = -\frac{D}{x_c} \ln \left[\frac{C_{cr}(K)}{C_0 K_S(K)} \right] = \frac{D}{x_c} \ln \left[\frac{C_{\infty}(K)}{C_{cr}(K)} \right] \quad (54)$$

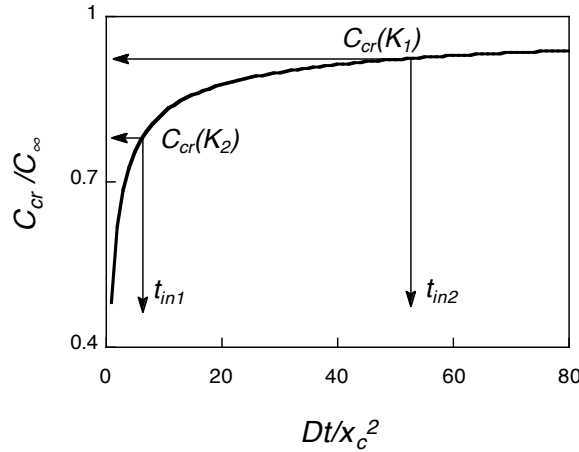


Fig. 28. Accumulation of hydrogen in a near-tip fracture site according to the solution of the diffusion problem for a stationary crack and a sketch to explain the tendency of change of the values of C_{cr} and t_{in} with variation of K (here $K_2 > K_1$).

The analysis clearly proves the intrinsic variability of crack growth rate values at a fixed K level, as shown in equation (52). Hence, in general, crack growth rate is not a single-value function of K , and the $v(K)$ -curve is not unique in a given {material-environment} system.

With regard to the *steady-state* regime of crack growth, all near-tip processes are time independent when viewed by an observer fixed to the moving crack tip. This obviously happens in HAC due to the existence of the steady-state solution (with $\partial C/\partial t = 0$ and $\partial v/\partial t = 0$) of the above considered coupled diffusion-cracking problem at constant K . The exact steady-state solution of equation (40) for a moving crack may be obtained using the same method as in the case of a stationary crack merely by nullifying the "fictitious driving force" (37), which yields the following:

$$C_{ss}(x_c; K, v) = C_0 K_S^*(x_c; K, v) \quad (55)$$

Comparing this with the estimate (50) of the non steady-state solution of the same equation, one may conclude that the approximate solution (50), at least, approaches at $t \rightarrow \infty$ the exact steady-state concentration distribution in the vicinity of a moving crack tip. That is, the formal approximation of the non steady-state solution (52) has the right asymptotic behaviour.

For a given {material-environment (hydrogen)} couple, the steady-state crack growth rate (54) is a single-value function of K , and thus the crack growth kinetics curve as a plot of v_{ss} vs. K possesses the uniqueness of a material's characteristic curve. This stage of the HAC process, the steady-state crack growth, appears to be really K -dominated.

Conclusions

Structural steels

The results of hydrogen embrittlement tests of pearlitic steel are strongly dependent on compressive residual stresses generated in the vicinity of the crack tip by fatigue pre-cracking, the relevant variable being the maximum stress intensity factor during the last stage of fatigue pre-cracking.

The threshold stress intensity value for hydrogen assisted cracking does not have an intrinsic character, but depends on the distribution of compressive residual stresses in the vicinity of the crack tip, and therefore on the fatigue pre-cracking level.

Fractographic analysis of hydrogen embrittlement tests on pre-cracked and notched samples of high-strength pearlitic steel reveals the existence of a special microscopic mode of fracture associated with hydrogen-induced micro-damage: the so called tearing topography surface or TTS.

Hydrostatic stress is the macroscopic variable governing the extension of the TTS zone. The hydrostatic stress distribution in notched samples is quasi-independent of the loading process, the point of maximum hydrostatic stress being a characteristic of the geometry.

The TTS depth is a function of test variables such as the electro-chemical potential, the maximum fatigue pre-cracking load and the test duration. These relations can be explained by means of a stress-assisted hydrogen diffusion model.

The role of diffusion as the main hydrogen transport mechanism in pearlitic steel is demonstrated by comparing the hydrogen affected region and the plastic zone. The hydrostatic stress plays an important role in accelerating hydrogen diffusion.

Hydrogen induced fracture in pearlitic steel notched samples is a time-dependent phenomenon, which allows a kinematic modeling of the process as a function of the strain rate. In this conceptual framework, the local strain rate in the vicinity of the notch tip is the relevant variable controlling the process.

In cold drawn prestressing steel wires, chemical modelling of hydrogen diffusion emphasizes the role of residual stresses generated in smooth wires during the manufacturing process.

In austenitic stainless steel notched samples, hydrogen damage consists of multi-cracking in the area surrounding the notch, and failure is produced by plastic instability, which allows a mechanical modelling of the action of hydrogen as a geometric enlargement of the notch in the form of extended micro-damage.

The notch extension model (NEM) is adequate from the mechanical point of view and is based on the assumption of a virtual damage in the form of a secondary notch whose depth is consistent with the elementary diffusion theory.

The notch cracking model (NCM) is adequate from the fractographic point of view and is based on the assumption of a virtual damage in the form of a secondary crack whose depth agrees fairly well with the real damage depth measured by quantitative fractography.

Progressively drawn steels

The steelmaking process by cold drawing to manufacture high-strength prestressing steel wires from a previously hot rolled pearlitic steel bar produces important microstructural changes in the material which could influence its engineering performance against environmentally assisted cracking.

In the framework of fracture mechanics, damage tolerance and structural integrity, a materials science approach was presented to link the microstructure of the steel with its macroscopic behaviour in corrosive environments promoting hydrogen assisted cracking or localized anodic dissolution.

The present approach links the progressively oriented microstructure of the steels as a consequence of the manufacture process by cold drawing with their macroscopic stress-corrosion behaviour which is increasingly anisotropic as the degree of cold drawing increases.

Fracture mechanics approach

The meaning and significance of the linear elastic fracture mechanics approach to hydrogen assisted cracking was revised for small scale yielding and stationary cracks under sustained or quasi-static loading.

The role of *far field* on near-tip diffusion of hydrogen is of minor importance and can affect the $v(K)$ -curve only in its near-threshold part, but it has no effect on the threshold itself which is still governed by K .

The effect of *history* appears in the form of coupling between hydrogen diffusion and crack growth and loss of K -dominance over the crack growth rate v , although a K -controlled steady-state value v_{SS} does exist.

Final conclusion

Since *material is itself and its circumstance*, when the latter is a hydrogenating environment, both far field and history (and especially the latter) could influence the coupled process of hydrogenation-cracking.

Therefore, in the matter of hydrogen assisted cracking, "the dream of yesterday is the hope of today and the reality of tomorrow" (R. H. Goddard), i.e., the yesterday affects the today, and the today influences the tomorrow.

In the latter case, it is possible to say, with the Spanish poet Antonio Machado, that "hoy es siempre todavía", and perhaps T. S. Eliot's "and all is always now".

Acknowledgements

The results summarized in this paper are taken from previous works reported in the list of references. Acknowledgement is gratefully given to the co-authors of such papers, and especially to Prof. Manuel Elices, Prof. Andrés Valiente, Dr. Ana María Lancha, Dr. Viktor Kharin, Dr. Elena Ovejero, the two latter being the co-authors of many papers on which this review is based.

References

- [1] J. Toribio, A. M. Lancha, M. Elices, Hydrogen embrittlement of pearlitic steels: phenomenological study on notched and precracked specimens, *Corrosion* 47 (1991) 781-791.
- [2] J. Toribio, A. M. Lancha, On the meaning of thresholds in environmentally assisted cracking, *J. Mater. Sci. Lett.* 11 (1992) 1085-1086.
- [3] J. Toribio, A. M. Lancha, Experimental evaluation of environmentally assisted cracking: the effect of compressive residual stresses at the crack tip, *J. Mater. Sci. Lett.* 14 (1995) 1204-1206.
- [4] J. Toribio, A. M. Lancha, M. Elices, Characteristics of the new tearing topography surface, *Scripta Metall. Mater.* 25 (1991) 2239-2244.
- [5] J. Toribio, A. M. Lancha, M. Elices, Macroscopic variables governing the microscopic fracture of pearlitic steels, *Mater. Sci. Engng. A* 145 (1991) 167-177.
- [6] J. Toribio, A. M. Lancha, M. Elices, The tearing topography surface as the zone associated with hydrogen embrittlement processes in pearlitic steel, *Metall. Trans.* 23A (1992) 1573-1584.
- [7] J. Toribio, Fracture mechanics approach to hydrogen-assisted microdamage in eutectoid steel, *Metall. Mater. Trans.* 28A (1997) 191-197.
- [8] J. Toribio, Hydrogen-assisted micro-damage evolution in pearlitic steel, *J. Mater. Sci. Lett.* 16 (1997) 1345-1348.
- [9] J. Toribio, Hydrogen-plasticity interactions in pearlitic steel: a fractographic and numerical study, *Mater. Sci. Engng. A* 219 (1996) 180-191.
- [10] J. Toribio, Role of hydrostatic stress in hydrogen diffusion in pearlitic steel, *J. Mater. Sci.* 28 (1993) 2289-2298.
- [11] J. Toribio, M. Elices, The role of local strain rate in the hydrogen embrittlement of round-notched samples, *Corros. Sci.* 33 (1992) 1387-1409.
- [12] J. Toribio, The role of crack tip strain rate in hydrogen assisted cracking, *Corros. Sci.* 39 (1997) 1687-1697.
- [13] J. Toribio, Material factors influencing notch tip strain rate, *Br. Corros. J.* 33 (1998) 23-28.
- [14] J. Toribio, Local strain rate at a crack tip: implications in stress corrosion cracking, *Br. Corros. J.* 32 (1997) 41-47.
- [15] J. Toribio, Numerical modelling of hydrogen embrittlement of cylindrical bars with residual stress fields, *J. Strain Anal.* 35 (2000) 189-203.
- [16] J. Toribio, M. Elices, Influence of residual stresses on hydrogen embrittlement susceptibility of pre-stressing steels, *Int. J. Solids Structures* 28 (1991) 791-803.
- [17] J. Toribio, Hydrogen embrittlement of prestressing steels: the concept of effective stress in design, *Materials & Design* 18 (1997) 81-85.
- [18] J. Toribio, Effects of strain rate and notch geometry on hydrogen embrittlement of AISI type 316L austenitic stainless steel, *Fusion Engng. Design* 16 (1991) 377-386.
- [19] J. Toribio, A. Valiente, R. Cortés, L. Caballero, Modelling hydrogen embrittlement in 316L austenitic stainless steel for the first wall of the Next European Torus, *Fusion Engng. Design* 29 (1995) 442-447.
- [20] A. Valiente, J. Toribio, R. Cortés, L. Caballero, Tensile failure of stainless steel notched bars under hydrogen charging. *ASME-J. Engng. Mater. Tech.* 118 (1996) 186-191.
- [21] J. Toribio, Experimental evaluation of micro-mechanical damage produced by hydrogen in 316L steel for the first wall of fusion reactors, *Fusion Engng. Design* 41 (1998) 85-90.
- [22] J. Toribio, R. Cortés, L. Caballero, A. Valiente, An integrated approach to the modelling of hydrogen assisted failure in 316L steel, *Fusion Engng. Design* 41 (1998) 91-96.
- [23] J. Toribio, E. Ovejero, Microstructure evolution in a pearlitic steel subjected to progressive plastic deformation, *Mater. Sci. Engng. A* 234-236 (1997) 579-582.
- [24] J. Toribio, E. Ovejero, Microstructure orientation in a pearlitic steel subjected to progressive plastic deformation, *J. Mater. Sci. Lett.* 17 (1998) 1037-1040.

- [25] J. Toribio, E. Ovejero, Effect of cumulative cold drawing on the pearlite interlamellar spacing in eutectoid steel, *Scripta Mater.* 39 (1998) 323-328.
- [26] J. Toribio, E. Ovejero, Effect of cold drawing on microstructure and corrosion performance of high-strength steel, *Mech. Time-Dependent Mater.* 1 (1998) 307-319.
- [27] J. Toribio, E. Ovejero, Micromechanics of hydro-gen assisted cracking in progressively drawn steels, *Scripta Mater.* 40 (1999) 943-948.
- [28] J. Toribio, E. Ovejero, Micromechanics of stress corrosion cracking in progressively drawn steels, *Int. J. Fracture* 90 (1998) L21-L26.
- [29] J. Toribio, V. Kharin, The reliability of the fracture mechanics approach to environmentally assisted cracking: 1. Uniqueness of the $v(K)$ -curve, *Mater. & Design* 18 (1997) 87-94.
- [30] J. Toribio, V. Kharin, The reliability of the fracture mechanics approach to environmentally assisted cracking: 2. Engineering safe design, *Mater. & Design* 18 (1997) 95-101.
- [31] J. Toribio, V. Kharin, Evaluation of hydrogen assisted cracking: the meaning and significance of the fracture mechanics approach, *Nucl. Engng. Design* 182 (1998) 149-163.
- [32] J. Toribio, V. Kharin, K -dominance condition in hydrogen assisted cracking: the role of the far field, *Fatigue Fract. Engng. Mater. Struct.* 20 (1997) 729-745.
- [33] J. Toribio, V. Kharin, The effect of history on hydrogen assisted cracking: 1. Coupling of hydrogenation and crack growth, *Int. J. Fracture* 88 (1997) 233-245.
- [34] J. Toribio, V. Kharin, The effect of history on hydrogen assisted cracking: 2. A revision of K -dominance, *Int. J. Fracture* 88 (1997) 247-258.